

LOCKHEED MARTIN ENERGY RESEARCH LIBRARIES



3 4456 0509607 1

ORNL/TM-5405

501

## Application of Hastelloy X in Gas-Cooled Reactor Systems

C. R. Brinkman  
P. L. Rittenhouse  
W. R. Corwin  
J. P. Strizak  
A. Lystrup  
J. R. DiStefano

OAK RIDGE NATIONAL LABORATORY  
CENTRAL RESEARCH LIBRARY  
DOCUMENT COLLECTION

### **LIBRARY LOAN COPY**

DO NOT TRANSFER TO ANOTHER PERSON

If you wish someone else to see this  
document, send in name with document  
and the library will arrange a loan.

UCN-7969  
(3 3-67)

# OAK RIDGE NATIONAL LABORATORY

OPERATED BY UNION CARBIDE CORPORATION FOR THE ENERGY RESEARCH AND DEVELOPMENT ADMINISTRATION

Printed in the United States of America. Available from  
National Technical Information Service  
U.S. Department of Commerce  
5285 Port Royal Road, Springfield, Virginia 22161  
Price: Printed Copy \$4.50; Microfiche \$2.25

This report was prepared as an account of work sponsored by the United States Government. Neither the United States nor the Energy Research and Development Administration/United States Nuclear Regulatory Commission, nor any of their employees, nor any of their contractors, subcontractors, or their employees, makes any warranty, express or implied, or assumes any legal liability or responsibility for the accuracy, completeness or usefulness of any information, apparatus, product or process disclosed, or represents that its use would not infringe privately owned rights.

ORNL/TM-5405  
Distribution  
Category UC-77

Contract No. W-7405-eng-26  
METALS AND CERAMICS DIVISION  
HTGR BASE PROGRAM  
(189a No. OH034)

APPLICATION OF HASTELLOY X IN GAS-COOLED REACTOR SYSTEMS

C. R. Brinkman, P. L. Rittenhouse, W. R. Corwin,  
J. P. Strizak, A. Lystrup, and J. R. DiStefano

Date Published: October 1976

OAK RIDGE NATIONAL LABORATORY  
Oak Ridge, Tennessee 37830  
operated by  
UNION CARBIDE CORPORATION  
FOR THE  
ENERGY RESEARCH AND DEVELOPMENT ADMINISTRATION

LOCKHEED MARTIN ENERGY RESEARCH LIBRARIES



3 4456 0509607 1



## CONTENTS

ABSTRACT . . . . .	1
INTRODUCTION . . . . .	1
MATERIAL CHARACTERIZATION . . . . .	3
ENVIRONMENTAL TEST FACILITIES . . . . .	7
Creep Test Facilities . . . . .	8
Fatigue Test Facility . . . . .	14
Subcritical Crack Growth Test Facility . . . . .	17
RESULTS . . . . .	20
Creep and Creep-Rupture Behavior . . . . .	20
Fatigue and Creep-Fatigue Interaction . . . . .	22
SUBCRITICAL CRACK GROWTH . . . . .	41
Thermal Stability . . . . .	44
Helium Corrosion . . . . .	46
SUMMARY AND CONCLUSIONS . . . . .	50
ACKNOWLEDGMENTS . . . . .	51
APPENDIX . . . . .	55



## APPLICATION OF HASTELLOY X IN GAS-COOLED REACTOR SYSTEMS

C. R. Brinkman, P. L. Rittenhouse, W. R. Corwin,  
J. P. Strizak, and A. Lystrup<sup>1</sup>

### ABSTRACT

Hastelloy X, an Ni-Cr-Fe-Mo alloy, may be an important structural alloy for components of gas-cooled reactor systems. Expected applications of this alloy in the High-Temperature Gas-Cooled Reactor (HTGR) are discussed, and the development of interim mechanical properties and supporting data are reported. Properties of concern include tensile, creep, creep-rupture, fatigue, creep-fatigue interaction, subcritical crack growth, thermal stability, and the influence of helium environments with controlled amounts of impurities on these properties. In order to develop these properties in helium environments that are expected to be prototypic of HTGR operating conditions, it was necessary to construct special environmental test systems. Details of construction and operating parameters are described. Interim results from tests designed to determine the above properties are presented. To date a fairly extensive amount of information has been generated on this material at Oak Ridge National Laboratory and elsewhere concerning behavior in air, which is reviewed. However, only limited data are available from tests conducted in helium. Comparisons of the fatigue and subcritical growth behavior in air between Hastelloy X and a number of other structural alloys are given.

### INTRODUCTION

Hastelloy X, an Ni-Cr-Fe-Mo alloy (nominally 47, 22, 19 and 9%, respectively, by weight), has been used successfully for more than two decades in a variety of elevated-temperature applications requiring high strength. It is essentially a single-phase alloy with a face-centered cubic structure and obtains its strength primarily by solid-solution strengthening from the elements Cr, Mo, and W. Some strengthening may also be due to the presence of carbide precipitates. Moreover, because of the high chromium content, it shows excellent resistance to oxidation to temperatures of about 982°C (1800°F) and higher. Perhaps its most

---

<sup>1</sup>On temporary assignment from the Danish Atomic Energy Commission, Metallurgy Department.

common usage has been in gas turbine engines, where it has been employed in sheet components. The specifications for this material are covered<sup>2,3</sup> in SB-435 of Sect. II and Sect. VIII of the ASME BPVC, and in Part 7 of ASTM Standards.<sup>4</sup> It is also approved for use to 900°C (1650°F) under Case 1321-2 (Special Ruling) to Sect. VIII, in unfired pressure vessels. Hastelloy X is not covered under Sect. III.

In the most recent design of the steam-cycle High-Temperature Gas-Cooled Reactor (HTGR), Hastelloy X was chosen for fabrication of the lower cross ducts, which connect the exit of the reactor core to the steam generators. Similarly, the upper cross ducts, which return the helium to the core, will also be constructed of Hastelloy X. A number of product forms (i.e., plate for the hot duct itself and its thermal barrier cover plates, sheet, bar, and forgings) are also of interest.<sup>5</sup> The nominal design temperature for the hot duct is 788°C (1450°F), with the possibility of temperature streaking (short term and random in position around the duct) up to 927°C (1700°F). Design lifetime is 280,000 hr in an environment of continuously recirculated and purified helium containing very low levels of impurity gases such as H<sub>2</sub>O, CO, CH<sub>4</sub>, and H<sub>2</sub>. The current technical specification limits the total content of oxidizing (oxygen-containing) species to 10 ppm with an upper design basis limit of about 500 ppm. The full-life fluence expected on the hot duct is no greater than 10<sup>18</sup> neutrons/cm<sup>2</sup>.

The design for the direct-cycle (gas turbine) HTGR also proposes the use of Hastelloy X, at a nominal temperature of 816°C (1500°F), in the ducts from the reactor core exit to the turbomachinery. Other design considerations for this use would be quite similar to those discussed above for the steam-cycle HTGR. Finally, Hastelloy X is one of the candidate materials for components of gas-cooled reactor process-heat plants (VHTR), which are expected to have application in the future for providing heat for coal conversion processes (e.g., hydrogasification, solution hydrocracking, and steam gasification), steel making, etc. In such systems, Hastelloy X might be used (depending upon temperature, stress, environment, etc.) for ducting or the tube or support-plate material of the intermediate and process-heat exchangers.

---

<sup>2</sup>ASME Boiler and Pressure Vessel Code, Section II: Materials Specifications, Part B - Nonferrous, The American Society of Mechanical Engineers, New York, 1971.

<sup>3</sup>ASME Boiler and Pressure Vessel Code, Section VIII: Pressure Vessels, Division 2 - Alternate Rules, The American Society of Mechanical Engineers, New York, 1971.

<sup>4</sup>1972 Annual Book of ASTM Standards, Part 7: Nonferrous Metals and Alloys; Electrodeposited Metallic Coatings; Metal Powders, Surgical Implants, American Society for Testing and Materials, Philadelphia, 1972.

<sup>5</sup>P. L. Rittenhouse, *Initial Assessment of the Status of HTGR Metallic Structural Materials Technology*, ORNL-TM-4760 (December 1974).

Use of Hastelloy X in the gas-cooled reactor systems mentioned above will require additional information and data on its mechanical behavior, thermal stability, and compatibility with helium and process environments. Our current work on Hastelloy X is specifically directed toward its use in the steam-cycle HTGR and includes efforts on:

1. creep and creep-rupture,
2. low-cycle fatigue and creep-fatigue interaction,
3. subcritical crack growth rates,
4. thermal stability,
5. helium corrosion and its effects on the items above.

In the sections which follow we summarize information currently available relative to each of the items above and describe the work now in progress.

### MATERIAL CHARACTERIZATION

The mechanical behavior of two product forms (plate and bar) is being evaluated in this program. Specific details concerning these materials are given in Table 1. Photomicrographs of samples from both heats are given in Fig. 1. Second-phase microconstituents are probably carbides of the  $M_6C$  type.

Table 1. Material Characterization

Product form:	13-mm (1/2-in.) plate	31.8-mm-diam (1 1/4-in.) bar
Heat No.	2600-3-4936	2600-3-2792
Source	Cabot-Stellite	Cabot-Stellite
ASME Specification	ASME SB-435 (N06002)	ASME SB-572 (N06002)
Heat treatment	Solution annealed at 1177°C (2150°F) followed by a rapid cool	Solution annealed at 1177°C (2150°F) followed by a rapid cool
Grain size	78 $\mu\text{m}$ (ASTM 4)	55 $\mu\text{m}$ (ASTM 5)
Hardness	DPH 190	DPH 197
	Chemical Composition, wt %	
Element	(plate)	(bar)
Ni	Bal	Bal
Cr	21.82	21.25
Fe	19.09	18.96
Mo	9.42	8.99
Co	1.68	1.94
W	0.63	0.56
Mn	0.58	0.57
Si	0.44	0.41
C	0.07	0.10
P	0.016	0.018
S	<0.005	<0.005
B	<0.002	<0.002

Y-139109

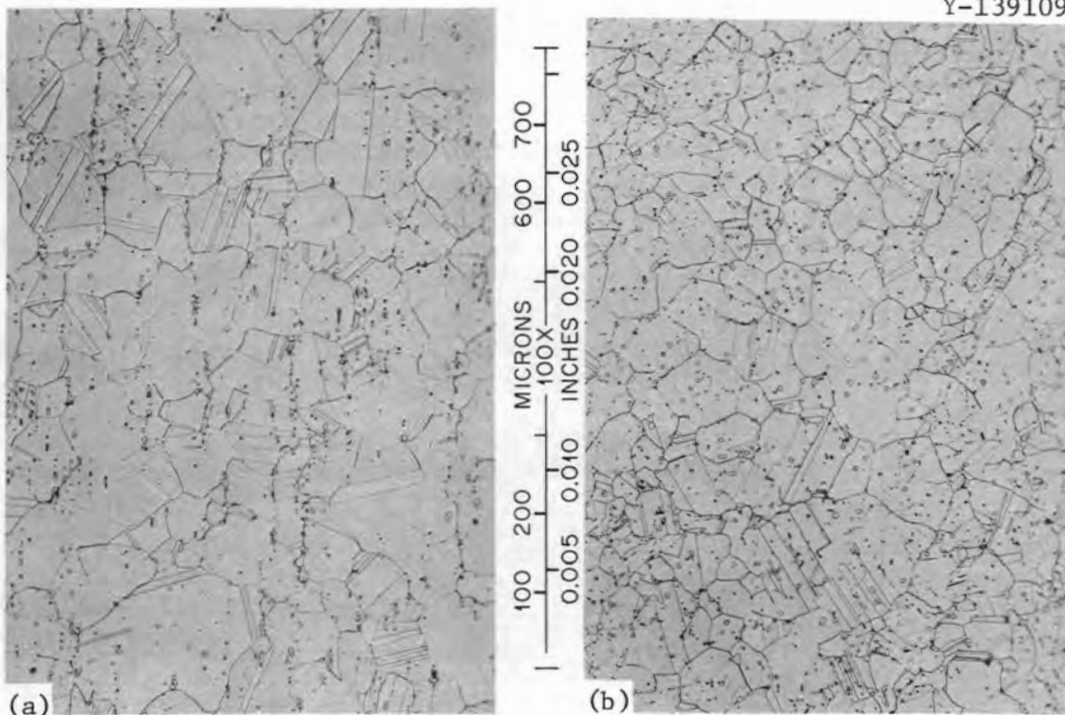


Fig. 1. Photomicrographs of Hastelloy X. (a) Heat No. 2600-3-4936, Plate. (b) Heat No. 2600-3-2792, Bar.

Tensile tests were conducted on heat 2600-3-4936. These tests were accomplished using specimens with a 6.35-mm-diam (0.25-in.) and 31.8-mm (1.25-in.) gage length. Tensile properties generated over the temperature range 20 to 870°C (70 to 1600°F) are given in Table 2, and are compared in Fig. 2 with tensile properties of other heats and product forms of Hastelloy X as given in the literature.<sup>6-9</sup> Figure 2 indicates that Hastelloy X shows a minimum in ductility as measured by reduction in area over the temperature range of about 500 to 750°C (932 to 1382°F). Such a ductility minimum is typical in nickel-base high-temperature alloys.<sup>10</sup>

<sup>6</sup>Hastelloy Alloy X, Technical Brochure, Cabot, Stellite Division, 1974.

<sup>7</sup>A. E. Carden and T. B. Slade, *High-Temperature Low-Cycle Fatigue Experiments on Hastelloy X*, Am. Soc. Test. Mater. Spec. Tech. Publ. 459, American Society for Testing and Materials, Philadelphia, 1968.

<sup>8</sup>E. L. Wagoner, *Physical Metallurgy and Mechanical Properties of Hastelloy Alloy X*, Haynes Stellite Company, Division of Union Carbide Corporation, Kokomo, Indiana, 1961.

<sup>9</sup>C. E. Jaske and T. L. Porfilio, *Low-Cycle Fatigue of Type 347 Stainless Steel and Hastelloy X in Hydrogen Gas Environment*, TID/SNA 2047, 1971.

<sup>10</sup>M. A. Arkoosh and N. F. Fiore, "Elevated Temperature Ductility Minimum in Hastelloy Alloy X," *Metall. Trans.* 3: 2235-2240 (August 1972).

Table 2. Tensile Properties of Hastelloy X  
Heat 2600-3-4936

Test No.	Temperature		Tensile strength				Elongation in 31.8 mm (1.25 in.), %		Reduction in area (%)
	(°C)	(°F)	0.2% Yield		Ultimate		Total	Uniform	
			(MPa)	(ksi)	(MPa)	(ksi)			
14892	20	70	359	52.0	762	110.5	50.5	43.8	59.8
14893	20	70	349	50.6	764	110.8	51.5	43.9	59.2
14894	20	70	350	50.8	764	110.8	51.9	44.3	61.4
14895	150	300	290	42.1	682	98.9	51.1	44.7	60.6
14899 <sup>a</sup>	150	300	288	41.8	671	97.3	51.5	45.9	59.8
14896	290	550	248	36.0	662	96.0	52.8	46.2	57.9
14897	290	550	244	35.4	651	94.4	53.7	48.3	55.9
14814	290	550	245	35.5	656	95.2	54.4	49.9	55.4
14812	430	800	223	32.4	627	91.0	56.5	51.1	56.9
14813	430	800	234	34.0	629	91.2	49.8	47.3	
14809	480	900	193	28.0	623	90.4	59.0	53.6	43.6
14810	480	900	234	34.0	622	90.2	55.9	53.0	38.4
14811	480	900	219	31.8	621	90.1	58.4	53.6	48.2
14807	540	1000	239	34.6	592	85.8	49.9	46.5	40.9
14808	540	1000	221	32.1	596	86.5	48.8	43.9	31.4
14804	595	1100	220	31.9	585	84.9	53.3	47.9	40.9
14805	595	1100	223	32.4	587	85.1	53.1	47.7	41.9
14806	595	1100	232	33.7	581	84.3	51.5	47.0	43.0
14802	650	1200	214	31.1	507	73.6	39.7	39.4	35.9
14803	650	1200	213	30.9	507	73.6	39.7	37.9	39.4
14799 <sup>a</sup>	705	1300	223	32.4	425	61.6	48.5	23.0	41.7
14800	705	1300	215	31.2	452	65.5	37.3	29.9	33.6
14801	705	1300	212	30.8	460	66.7	37.6	30.8	35.9
14790 <sup>a</sup>	760	1400	215	31.2	320	46.4	73.3	6.4	66.1
14791 <sup>a</sup>	760	1400	217	31.5	323	46.9	75.6	7.8	68.8
14796	760	1400	217	31.5	385	55.8	66.6	11.7	55.8
14798	760	1400	206	29.9	381	55.2	68.1	12.0	57.0
14792 <sup>a</sup>	815	1500	221	32.1	241	34.9	87.2	3.0	78.9
14793 <sup>a</sup>	815	1500	232	33.7	240	34.8	72.2	3.4	74.3
14794 <sup>a</sup>	815	1500	231	33.5	238	34.5	74.6	3.2	77.1
14795 <sup>a</sup>	815	1500	213	30.9	241	34.9	81.2	3.2	81.4
14797	815	1500	225	32.7	288	41.7	86.0	5.8	69.6
14815 <sup>a</sup>	870	1600	161	23.4	165	24.0	79.8	2.1	88.9
14898 <sup>a</sup>	870	1600	163	23.6	168	24.3	84.4	2.3	88.2

<sup>a</sup>Constant strain rate of 0.4%/min through failure. All other tests at this rate through yielding and then increased by factor of 4.

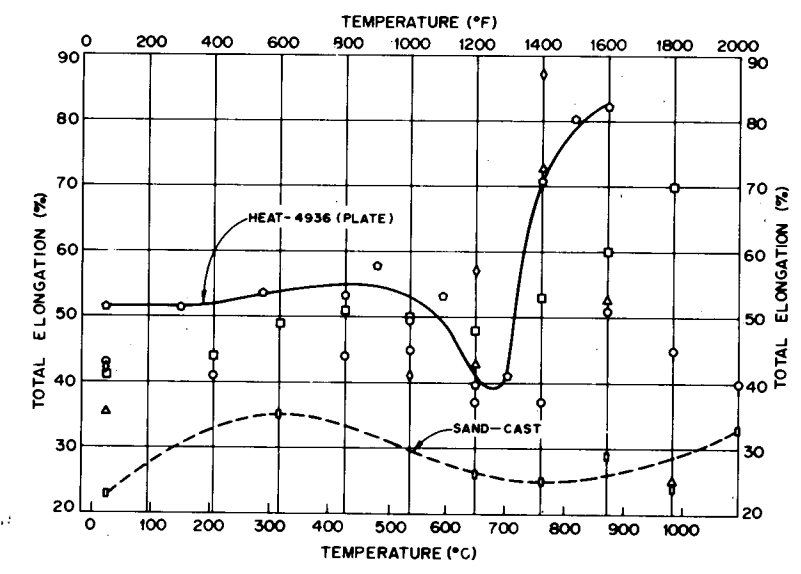
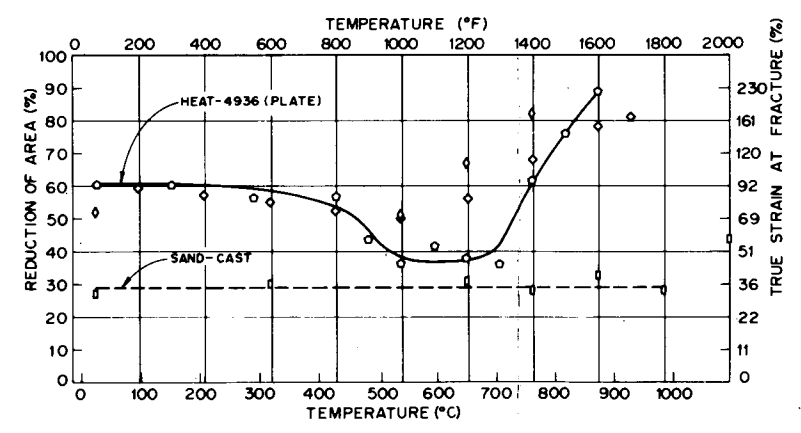
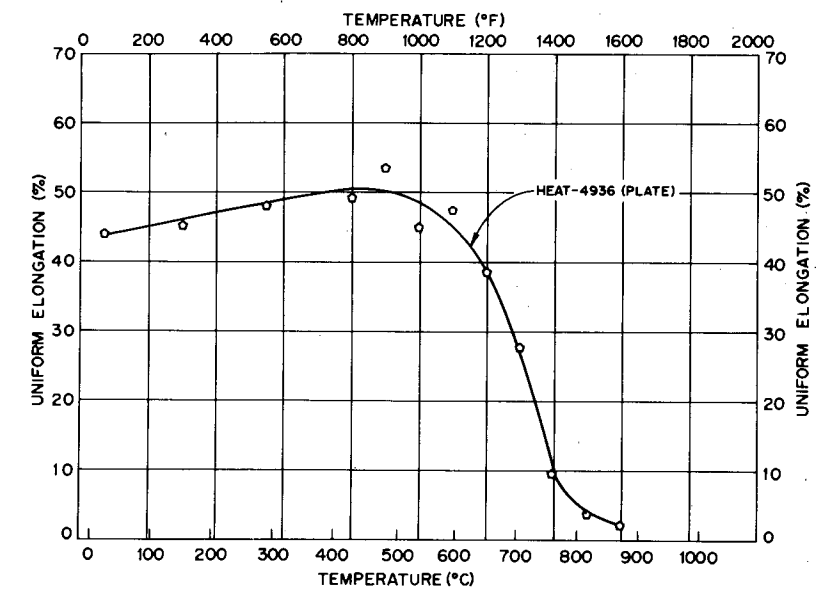
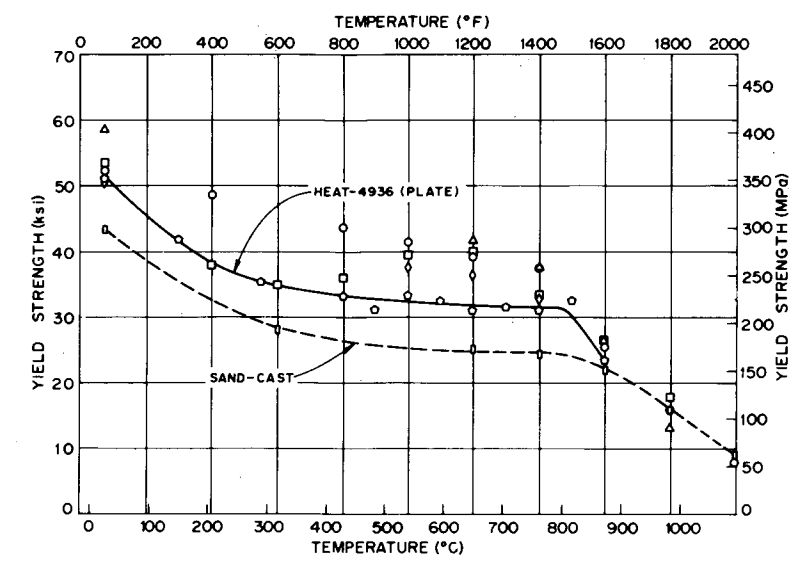
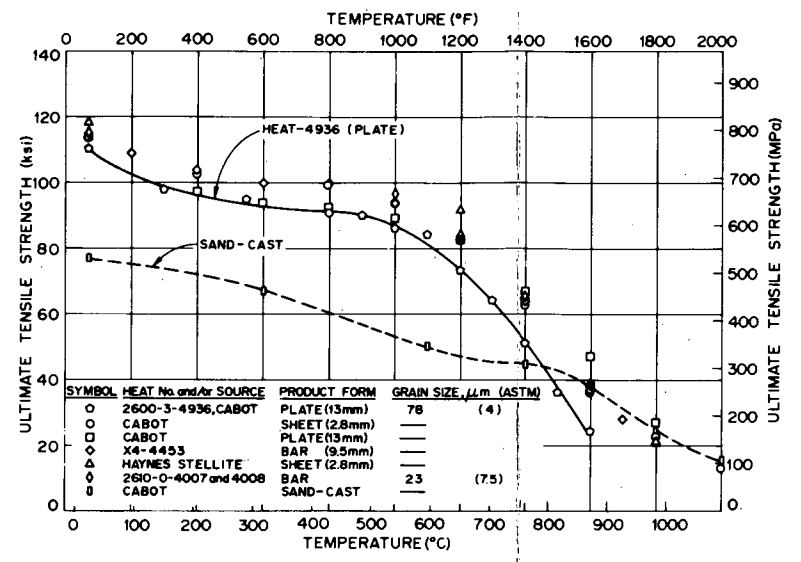


Fig. 2. Comparison of the Tensile Properties for Hastelloy X as a Function of Temperature.

## ENVIRONMENTAL TEST FACILITIES

It is well established that the fatigue and creep-rupture properties of engineering alloys can be affected by operation at elevated temperatures in gaseous media.<sup>11-15</sup> For engineering purposes the magnitude of the effect may be large or small, depending upon the nature of the surface film formed, the surface-to-volume ratio of the components, and the type of loading involved, that is, static or dynamic. The extent of reaction can be particularly pronounced if the environment acts as a mass transfer agent for oxidation, decarburization, or carburization. These reactions can be particularly deleterious if intergranular attack occurs, since grain boundaries tend to be weak at elevated temperatures. In air environments the primary oxide to form on Hastelloy X is a smooth adherent scale of  $\text{Cr}_2\text{O}_3$  which remains stable and protective until temperatures of about  $982^\circ\text{C}$  ( $1800^\circ\text{F}$ ) are exceeded.<sup>16</sup> This adherent oxide makes Hastelloy X an excellent material for elevated-temperature applications in air. Above about  $982^\circ\text{C}$  ( $1800^\circ\text{F}$ ) a volatile oxide product,  $\text{CrO}_3$ , forms which is nonprotective.<sup>16</sup>

The primary coolant of the HTGR, on the other hand, is helium, and it contains only small quantities of oxidizing species, as indicated in Table 3. Therefore the nature (i.e., adherent or exfoliating) of surface films or corrosion products that may develop as a consequence of prolonged exposure (280,000 hr) to environments given in Table 3 needs to be determined. Since current ASME elevated-temperature design allowables are based on mechanical properties such as tensile, creep, and fatigue

---

<sup>11</sup>H. E. McCoy, "Type 304 Stainless Steel vs Flowing  $\text{CO}_2$  at Atmospheric Pressure and 1100-1800 F," *Corrosion* 21 84-94 (1965).

<sup>12</sup>C. P. Sullivan and M. J. Donachie, Jr., "Microstructure and Mechanical Properties of Iron-Base (-Containing) Superalloys," *Met. Eng. Q.* 11(4): 1-9 (November 1971).

<sup>13</sup>F. S. Pettit and J. K. Tien, "Hot Gas Environment - Alloy Reactions and Their Relation to Fatigue," *Corrosion Fatigue: Chemistry, Mechanics and Microstructure*, National Association of Corrosion Engineers, NACE-2, 1972, pp. 576-89.

<sup>14</sup>G. W. Titus and W. L. Clarke, Jr., "Compatibility of Reactor Materials with High-Temperature Gases," *Nucl. Eng. Des.* 24: 125-44 (1973).

<sup>15</sup>D. S. Wood, M. Farrow, A. B. Baldwin, and W. T. Burke, "Creep Rupture Properties of Some High Temperature Reactor Circuit Materials in Helium," pp. 158.1-158.9 in *Int. Conf. Creep and Fatigue in Elevated Temperature Applications*, *Inst. Mech. Eng. Conf. Publ.* 13, Institution of Mechanical Engineers, London, 1973.

<sup>16</sup>J. S. Brunhouse and G. W. Titus, *Evaluation of Long-Term Gas Corrosion of Heat Resistant Alloys for Use as Gas-Cooled Reactor Fuel Cladding*, USAEC Research and Development Report IDO-28605 (1963).

that were generated in air, the impact of HTGR prototypic environments on these properties must be defined for design purposes. Toward this end, facilities for determining creep, subcritical crack growth, and strain-controlled fatigue behavior in HTGR prototypic environments were or are currently being developed and will be discussed in the following sections.

Table 3. Estimated Impurity Levels  
in Gas-Cooled Reactor Helium

Impurity	Impurity levels, $\mu\text{atm}$		
	Minimum <sup>a</sup>	Expected <sup>b</sup>	European <sup>c</sup>
H <sub>2</sub> O	<1	50	d
CH <sub>4</sub>	20	50	20-50
CO	10	450	2-50
CO <sub>2</sub>	<1	<2	
H <sub>2</sub>	200	1500	100-500
O <sub>2</sub>	10 <sup>-19</sup>	10 <sup>-16</sup>	$\leq 10^{-3}$
N <sub>2</sub>	<1	<1	<10

<sup>a</sup>General Atomic Company estimate for totally leak-free steam generator at equilibrium after startup.

<sup>b</sup>Estimate based on General Atomic Company technical specification limits.

<sup>c</sup>Based on discussions with Dragon Project and UKAEA.

<sup>d</sup>Strongly dependent on time in life, reactor design, etc.

### Creep Test Facilities

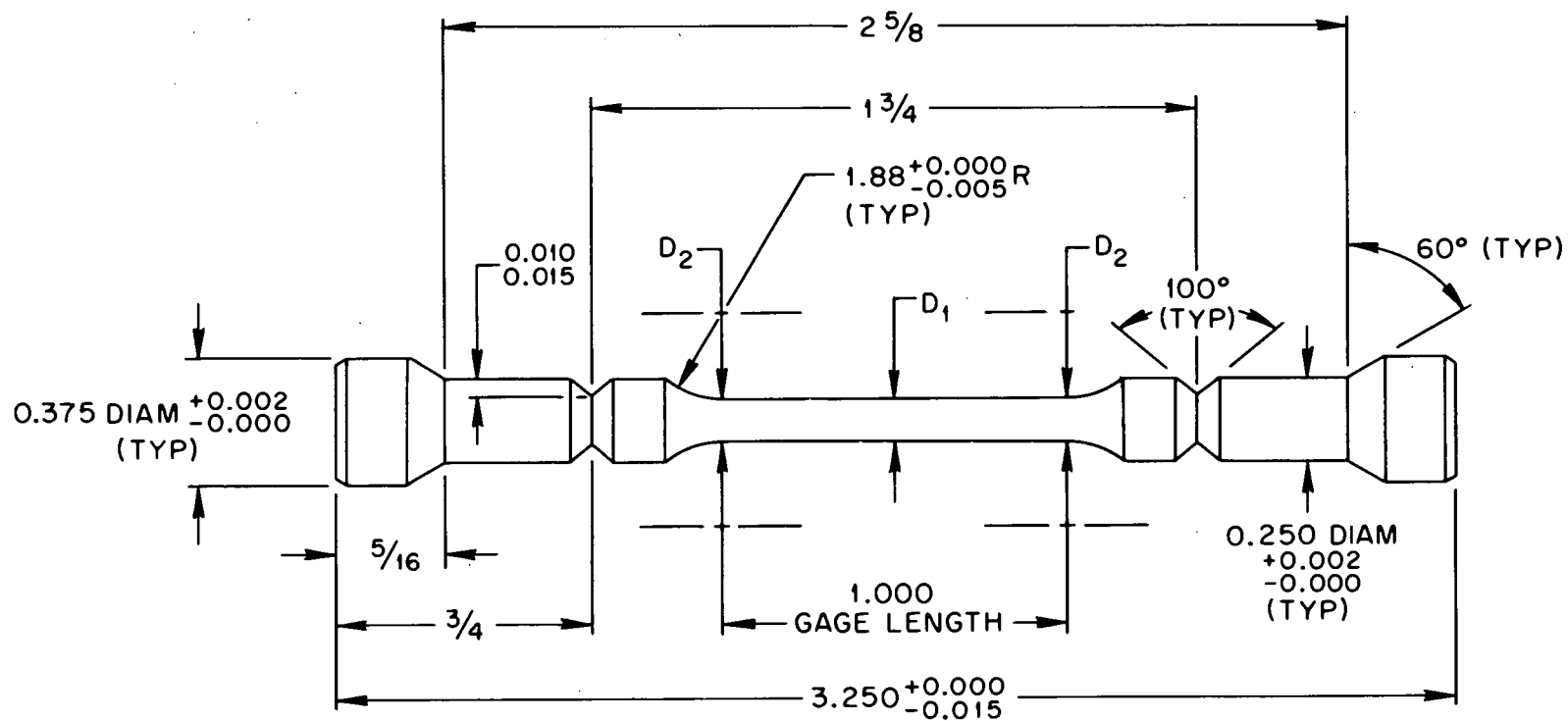
Conventional high-precision creep testing (i.e., in air) involves, in brief, load train systems for applying uniaxial loads with a minimum of bending stresses, extensometry to monitor the strain which accrues with time, and furnaces and controls for maintaining the desired test temperature within narrow limits for long periods of time. Testing in a controlled environment adds substantially to the above in complexity, effort, and cost. The ten systems we are now using for environmental tests required extensive development related to the design of the specimen, load train, extensometry, environmental chamber, and, particularly, to the methods for supplying and monitoring the helium environments. Six frames were also built for testing of control specimens in air.

Loading of the creep specimens is provided conventionally through calibrated lever arms. The load train itself is designed to minimize bending loads by the use of universal joints and the elimination of threaded connections. This practice is carried over to the specimens (see Fig. 3) by attaching them to the load train with tapered fittings clamped over each end. The environmental chamber (Fig. 4) is constructed of austenitic stainless steel pipe (enclosed in the furnace bore) with water-cooled flanges and metal bellows at each end. The bellows are provided to further facilitate alignment of the load train. U-cup seals, lightly lubricated to minimize friction, are used where the polished pull rods enter and exit the environmental chamber. This allows a positive environmental seal and, yet, permits application of load and unrestricted specimen extension. Seals are also used where the extensometer rods are led through the bottom of the chamber. The bores of the environmental chambers are seasoned (preoxidized) prior to use.

Three Chromel-Alumel thermocouples are attached equidistantly along the specimen gage length to monitor temperature. The three-zone furnace surrounding the environmental chamber bore is shunted to achieve a maximum of  $2^{\circ}\text{C}$  ( $3.6^{\circ}\text{F}$ ) difference over the 25.4-mm (1-in.) gage length. The control thermocouple is placed in the annulus between the chamber and the furnace to avoid any possibility of reaction between the thermocouple materials and the helium environment that would lead to possible changes in thermocouple output. Before any test specimen is brought to temperature and loaded, the environmental chamber is evacuated and then backfilled with helium.

Provision of a system for supplying, monitoring, and controlling the simulated HTGR primary-coolant helium environment has been the most difficult step in facility preparation. The three types of systems considered are (1) premixed (tank) gas supply, (2) once-through dynamic-mix supply, and (3) recirculating-loop dynamic-mix supply. The first (premixed) can be provided at the lowest cost and is the most versatile system; however, it does not offer continuous on-line control of purity levels. Early concerns relative to gas stability (i.e., possible changes in impurity levels in the tanks during storage and use) and cleanliness were, and continue to be, dispelled by our experience in the use of this method. Prior to adopting this method of supply, tanks containing controlled additions of  $\text{H}_2 + \text{CO} + \text{CH}_4$  to helium were prepared and bled from 1000 psia to 50 psia over a 600-hr period. (A normal period for tank use in test is  $<300$  hr). No changes in impurity levels were detected during this period. A schematic of the premixed system is shown in Fig. 5.

Once-through dynamic-mix systems can provide simulated HTGR primary-coolant helium by continuous additions of  $\text{H}_2$ , etc. (through micrometering valves), to high-purity helium. Such systems are intermediate in cost and versatility. Construction of such a system is in progress and is shown schematically with the premixed system in Fig. 6. We have also considered dynamic-mix recirculating loops which are attractive from



NOTE: ALL DIMENSIONS IN INCHES

$D_1 = 0.125 \pm 0.001$  DIAM

$D_2 =$  FROM 0.0010 TO 0.0015  
GREATER THAN  $D_1$

Fig. 3. Environmental Creep Test Specimen. 1 in. = 25.4 mm.

ORNL-DWG 76-2207R

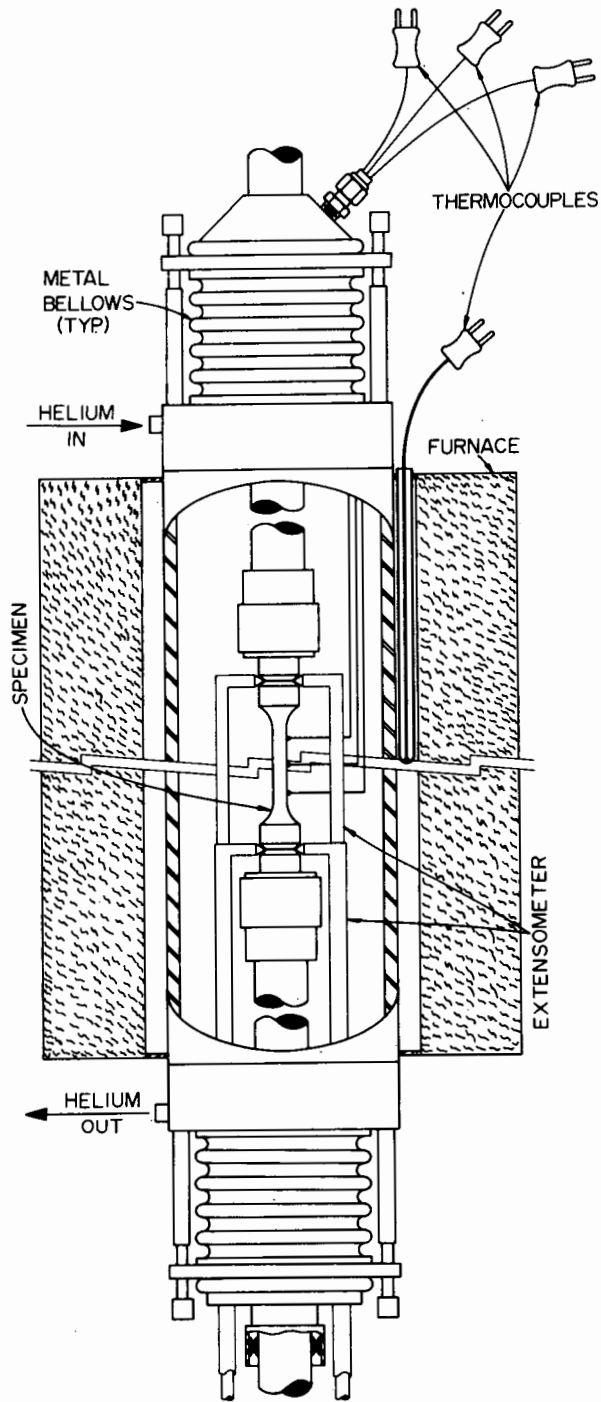


Fig. 4. Creep Environmental Test Chamber.

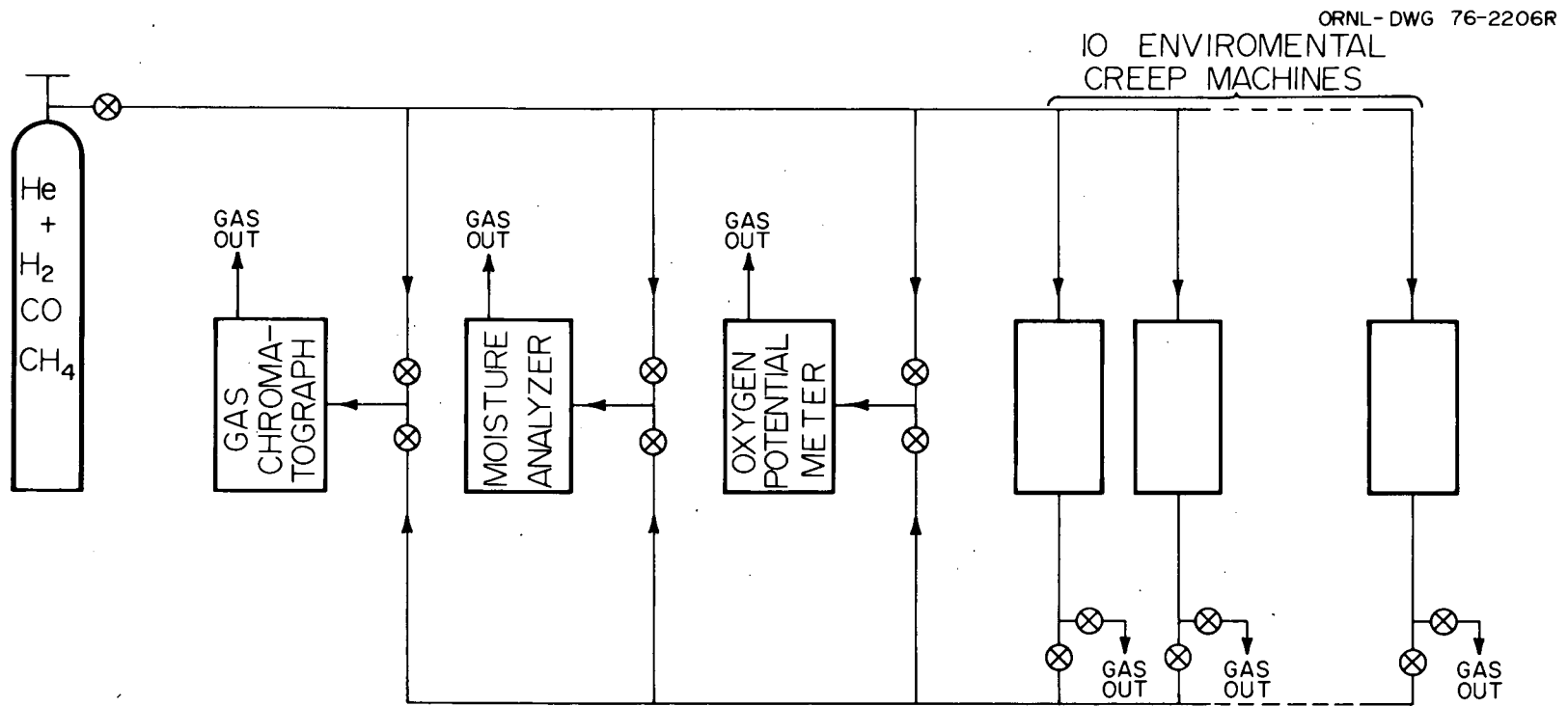


Fig. 5. Schematic of the Premixed Gas Supply System.

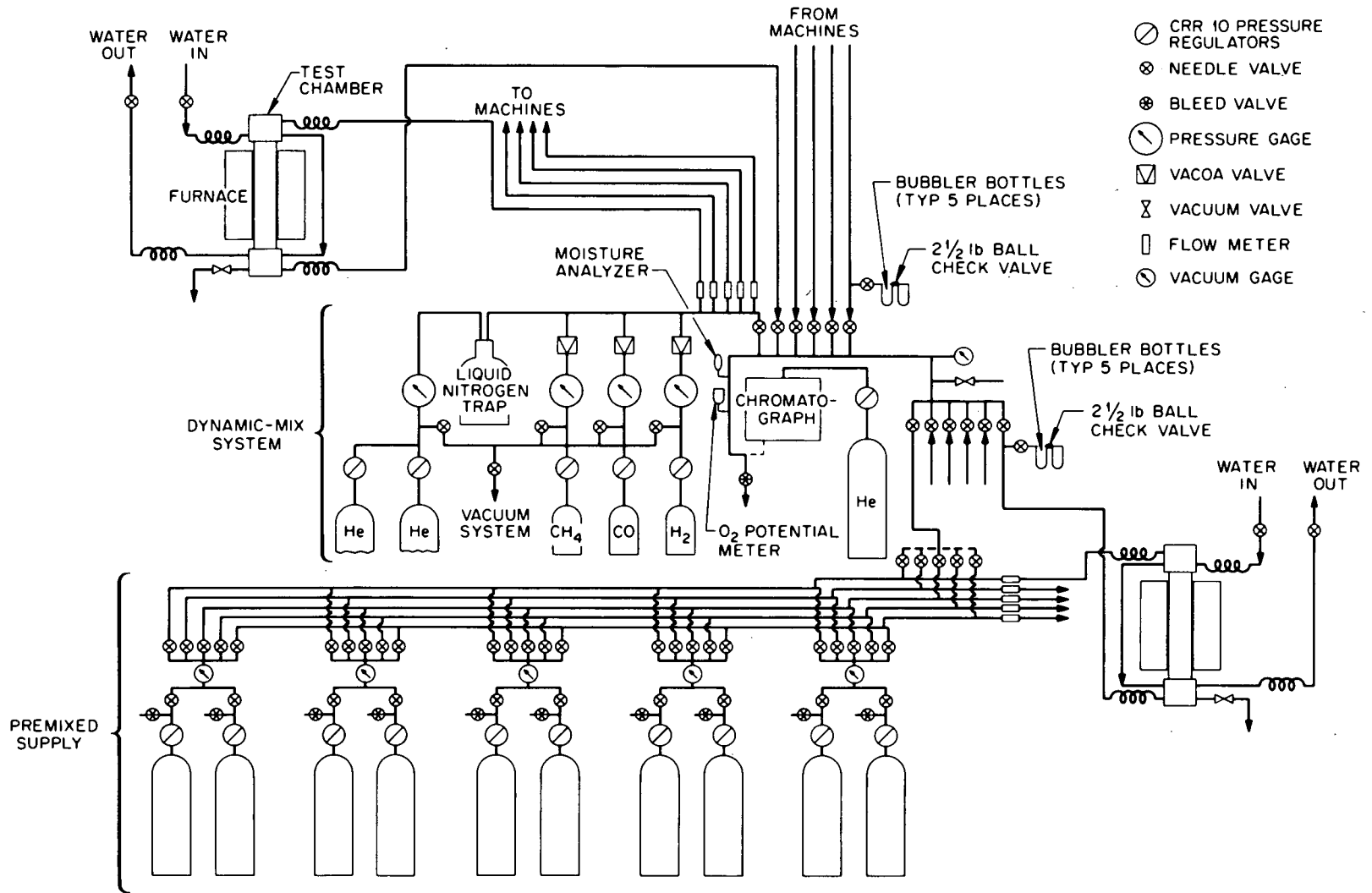


Fig. 6. Schematic of the Dynamic and Premixed Gas Supply System.

the standpoint of helium costs and long-term stability of the helium environment. These systems are, however, of minimum versatility, and their construction costs far exceed those which could be considered in our program.

The impurity levels in the helium supply are monitored entering and leaving the environmental creep chambers. The H<sub>2</sub>, CO, and CH<sub>4</sub> levels are measured using a gas chromatograph. The chromatograph offers an additional leak-check feature by indicating N<sub>2</sub> level. Water vapor content of the gas is followed with a separate moisture analyzer, and a solid-state oxygen potential meter is used as the oxygen partial pressure reference.

Until now the environment for all tests has been supplied from premixed tanks containing controlled additions of H<sub>2</sub>, CO, and CH<sub>4</sub>. System pressure is normally 1.1 to 1.2 atm, and the gas flow through the chambers ranges from 30 to 50 cm<sup>3</sup>/min.

Impurity levels in the simulated HTGR primary-coolant helium before entering and after leaving the environmental chambers are typified by the values given in Table 4. Differences between the inflowing and effluent gas concentrations are due to metal-gas reactions occurring within the system. Comparison of the gas impurity levels given in Table 4 with the estimated impurity levels expected in steam-cycle gas-cooled reactors (Table 3) indicates that the test environments are appropriate.

Table 4. Impurity Levels in the Simulated HTGR Primary-Coolant Helium Before Entering and After Leaving the Creep Machines.

Impurity	Entering content ( $\mu\text{atm}$ ) <sup>a</sup>	Leaving content ( $\mu\text{atm}$ ) <sup>a</sup>
H <sub>2</sub>	250-300	230-290
CH <sub>4</sub>	25-30	20-30
CO	15-25	10-15
H <sub>2</sub> O	2-7	10-25
O <sub>2</sub>	<10 <sup>-15</sup>	<10 <sup>-15</sup>

<sup>a</sup>  $\mu\text{atm} = \text{ppm by volume} \times \text{system pressure}$  (1  $\mu\text{atm} = 1 \text{ ppm}$  at 1 atm).

#### Fatigue Test Facility

A schematic diagram of the vacuum and environmental fatigue test chamber under construction is shown in Fig. 7. Upon completion this chamber will be connected to the gas analysis and supply system discussed previously. Therefore, no tests have been conducted to date in helium

ORNL - DWG - 76 - 1831

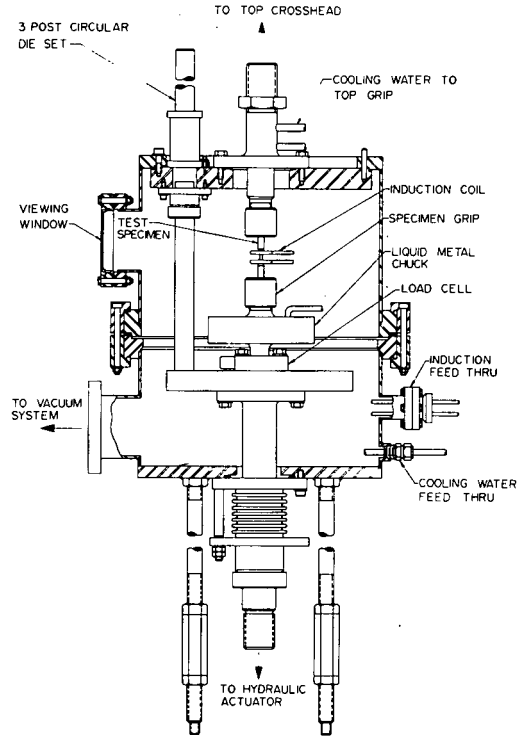


Fig. 7. Schematic of Vacuum and Environmental Fatigue Test Chamber.

with controlled impurity levels; however, considerable baseline data generated in air at elevated temperatures have been obtained.

Fully reversed axial push-pull testing is accomplished in closed-loop electrohydraulic fatigue test machines (Fig. 8). Axial strain control is maintained by employing a diametral extensometer and a simple diametral-to-axial strain computer. Total strain range,  $\Delta\epsilon_t$ , was thus determined by the relation

$$\Delta\epsilon_t = (\Delta\sigma/E)(1 - 2\nu) + 2\Delta\epsilon_d, \quad (1)$$

where  $E$  is Young's modulus,  $\nu$  is Poisson's ratio,  $\Delta\epsilon_d$  is the diametral strain range, and  $\Delta\sigma$  is the peak-to-peak stress range from the hysteresis loops.

A schematic drawing of a fatigue specimen is shown in Fig. 9. Specimens were heated by induction in air, with thermocouples attached to the specimens some distance from the point of minimum diameter. Tests were conducted at several temperatures ranging from room temperature to 871°C (1600°F).

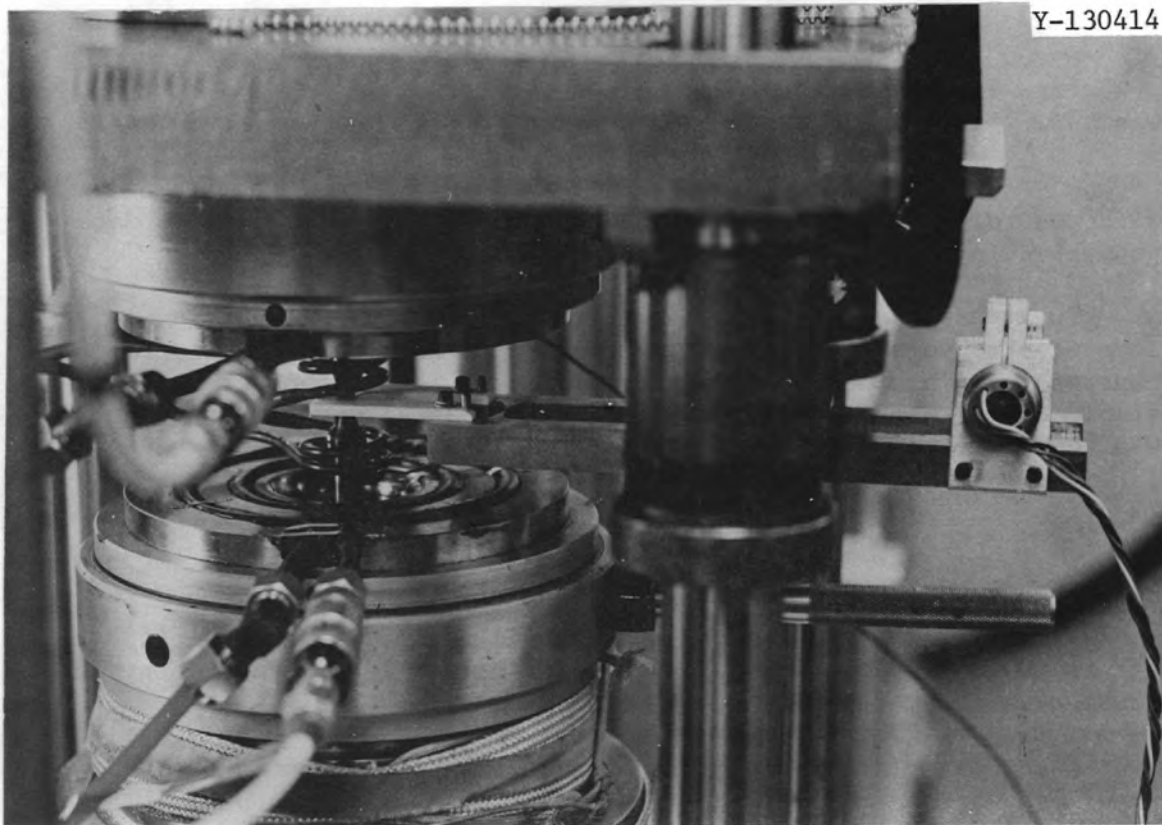
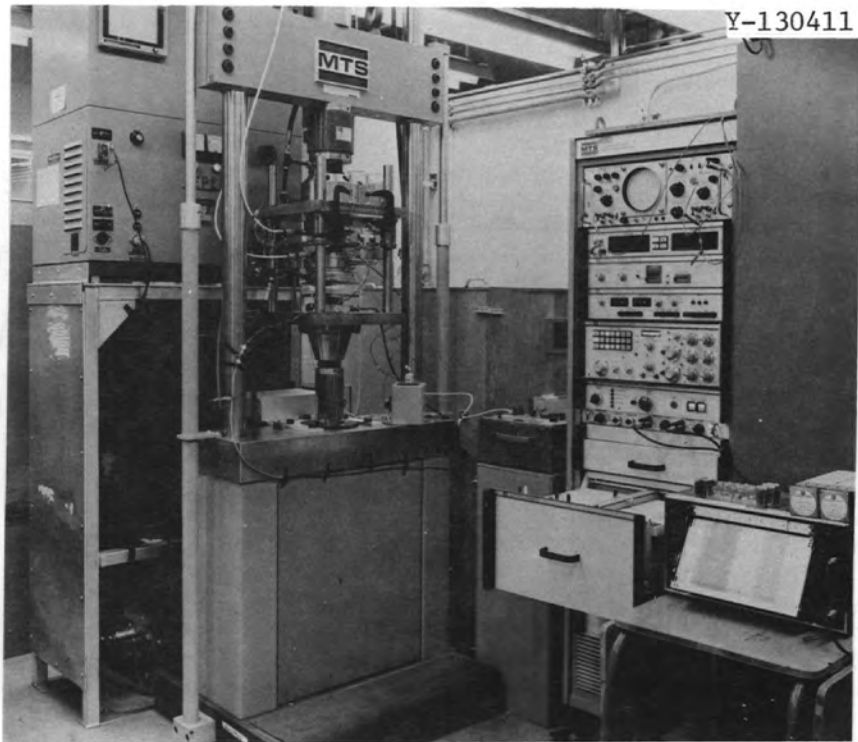


Fig. 8. Typical Strain-Controlled Fatigue System Used at ORNL for Elevated-Temperature Fatigue Testing.

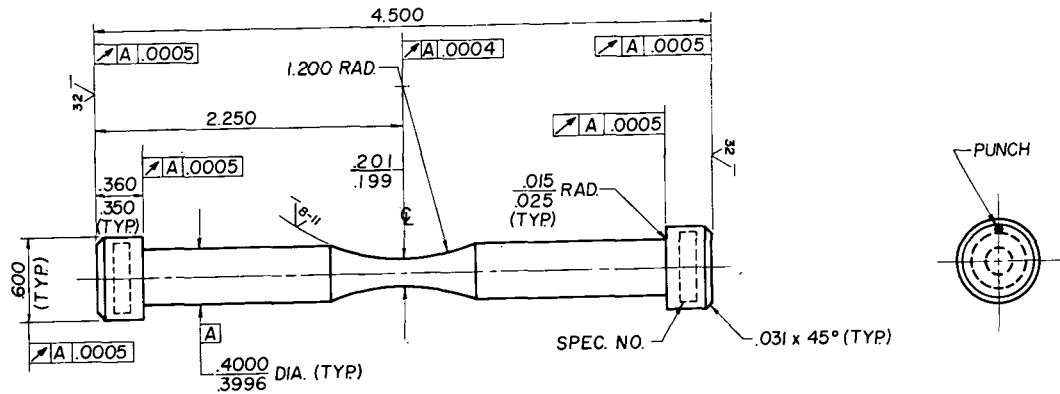


Fig. 9. Fabrication Drawing Showing Details of Fully Reversed Strain- or Load-Controlled Fatigue Specimen. All dimensions are in inches (1 in. = 25.4 mm).

#### Subcritical Crack Growth Test Facility

Subcritical crack growth tests were conducted both in air and in an environmental chamber shown in Fig. 10. The gas supply and analysis system is essentially the premixed type shown in Fig. 5, and helium gas impurity levels are comparable to those given in Table 4.

Two specimen geometries were employed for subcritical crack growth testing: the compact tension specimen ( $h/w = 0.60$ ) and the wedge opening load (WOL) specimen ( $h/w = 0.48$ ) (see Fig. 11). The small compact tension specimen was chosen since it could be conveniently tested in an existing vacuum furnace, while the WOL specimen was selected as the reference specimen for most of the crack growth studies in air, since its longer length permits a lower rate of change of stress intensity factor with crack length, and more data can be collected from a given test. The stress intensity expression used for the WOL specimen was as follows:

$$\Delta K = (\Delta P \sqrt{a/Bw}) [30.96 - 195.8(a/w) + 730.6(a/w)^2 - 1186.3(a/w)^3 + 754.6(a/w)^4] , \quad (2)$$

where

- $B$  = specimen thickness,
- $\Delta P$  = cyclic load change,
- $w$  = specimen width,
- $a$  = crack length measured from the centerline of loading to the crack tip.

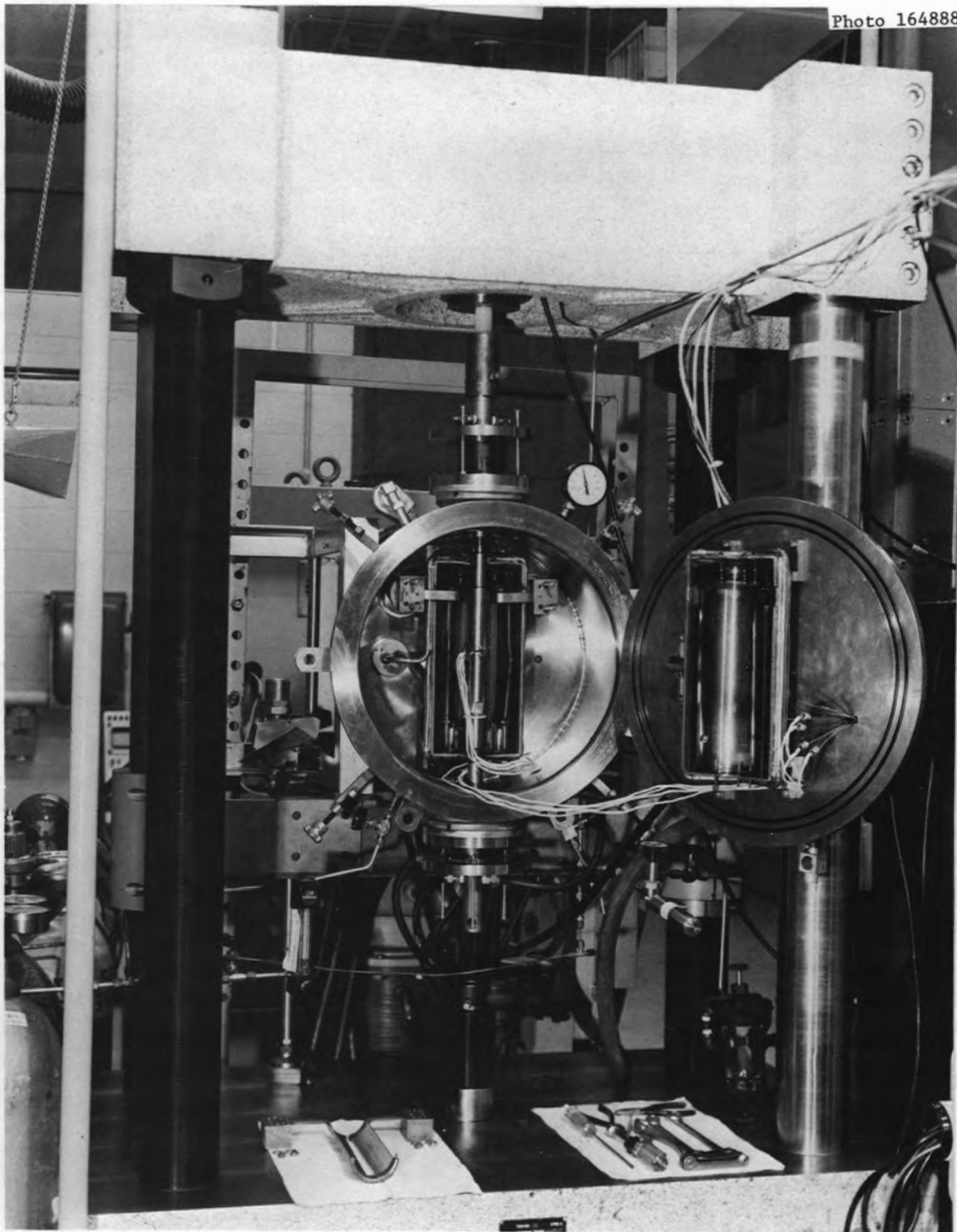


Fig. 10. Environmental Chamber Used for Conducting Subcritical Crack Growth Tests in Either Helium or Vacuum.

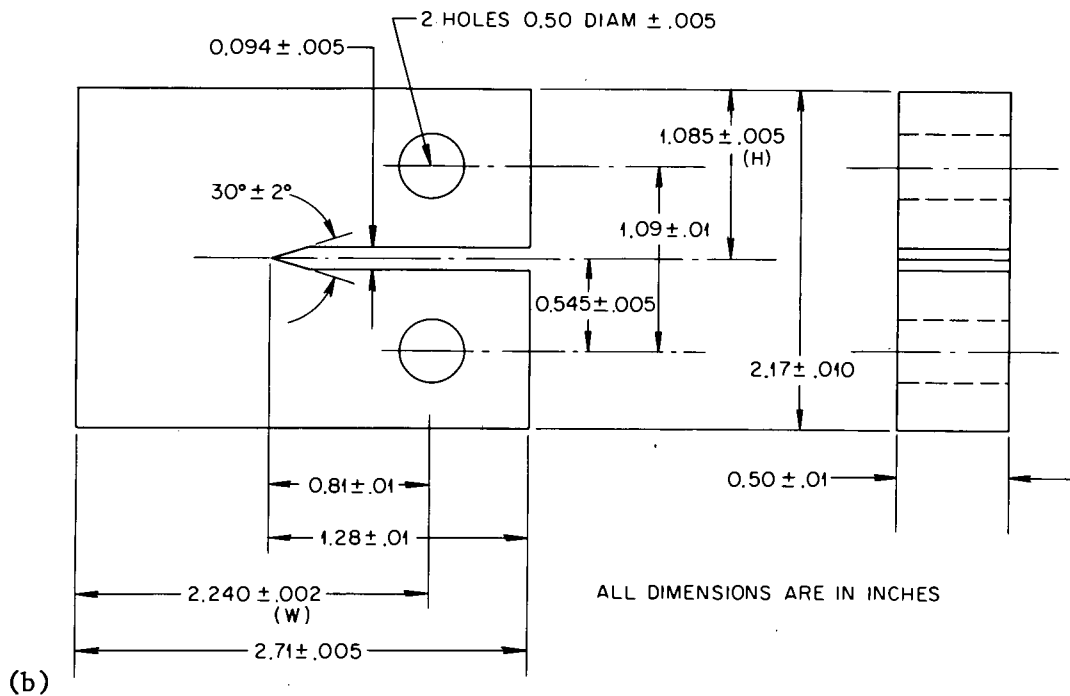
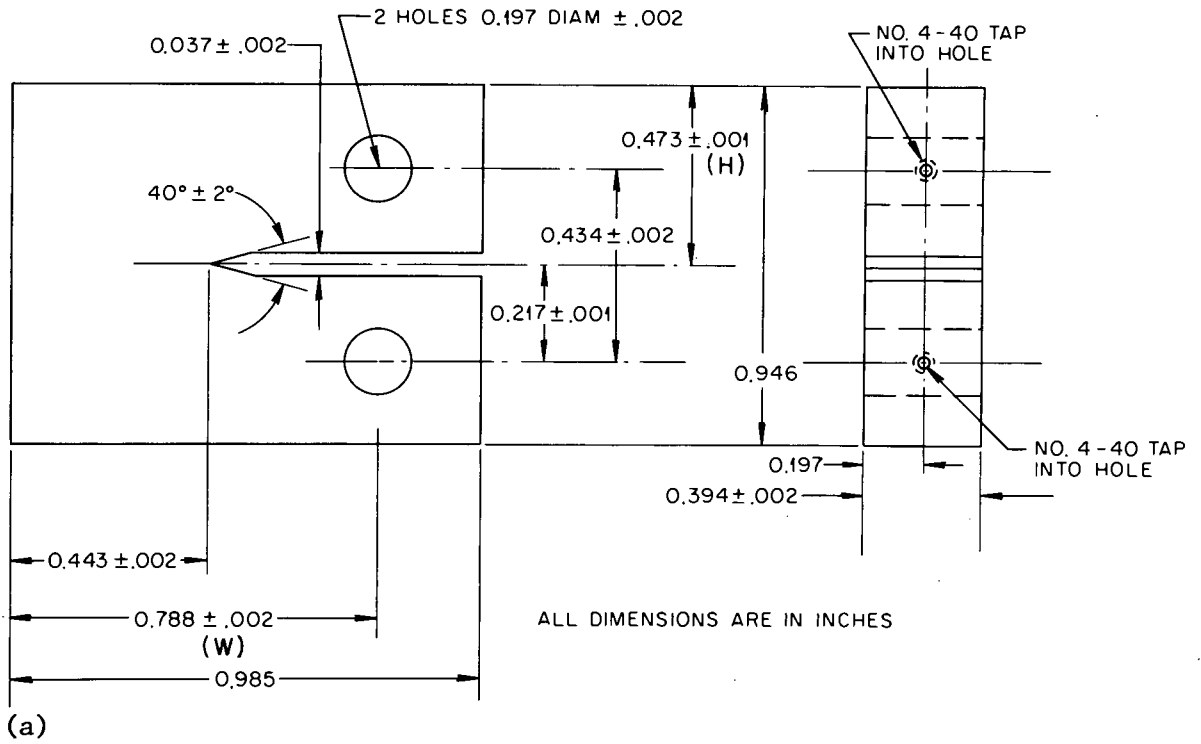


Fig. 11. Details of Specimens Used in Crack Growth Studies. All dimensions are in inches (1 in. = 25.4 mm). (a) Compact tension specimen. (b) WOL specimen.

The stress intensity expression used for the compact tension specimen was as follows:

$$\Delta K = (\Delta P/B \sqrt{w}) [29.6(a/w)^{0.5} - 185.5(a/w)^{1.5} + 655.7(a/w)^{2.5} - 1017(a/w)^{3.5} + 638.9(a/w)^{4.5}] \quad (3)$$

We calculated  $da/dN$  vs  $\Delta K$  from recorded  $a$  vs  $N$  data ( $N$  = number of cycles) with a computer, using a first-order forward divided difference technique. For any two successive data points  $(a_i, N_i)$  and  $(a_{i+1}, N_{i+1})$ , crack growth rate was computed by

$$\frac{da}{dN} = \frac{a_{i+1} - a_i}{N_{i+1} - N_i} \quad (4)$$

This equation gives the average value of  $da/dN$  between cycles  $N_i$  and  $N_{i+1}$ .

The associated  $\Delta K$  for the same cycle increment is computed by use of the simple arithmetic mean of the crack length during that increment:

$$a_{av} = (a_i + a_{i+1})/2 \quad (5)$$

This value of  $a_{av}$  is then used with the appropriate stress intensity factor expressions given above.

## RESULTS

### Creep and Creep-Rupture Behavior

Currently, only limited creep and creep-rupture data are available from tests conducted in a simulated HTGR environment, and no data for comparison purposes are available from tests conducted in air on identical material, that is, the same heat. Comparison air data will be available in the near future, and in the interim it was thought to be instructive to compare simulated HTGR environment rupture data with data available in the literature.<sup>17-19</sup> Table 5 gives the results of tests conducted

<sup>17</sup>Hastelloy Alloy X, Technical Brochure, Cabot, Stellite Division, 1974.

<sup>18</sup>J. W. Tackett, *The Creep Rupture Properties of Hastelloy Alloy X Sheet*, Tech. Dept. Report No. 8745, Stellite Division, Cabot, Corporation, Kokomo, Indiana, 1975.

<sup>19</sup>Component and Systems Development Program Q. Prog. Rep. Dec. 31, 1975, General Atomic Project 3218, GA-A13778

Table 5. Interim Results of ORNL Creep-Rupture Tests on Hastelloy X in Progress or Completed.

Test No.	Heat No.	Temperature		Stress		Rupture Life (hr)	Elongation (%)	Steady-State Creep Rate (hr <sup>-1</sup> )	Environment	Time-to-Tertiary Creep (hr)
		(°C)	(°F)	(MPa)	(ksi)					
15772	2600-3-4936	649	1200	172	25	6466	34.9	$1.66 \times 10^{-5}$	He	3950
16267	2600-3-4936	649	1200	172	25	In progress	In progress		Air	
17329	2600-3-4936	649	1200	138	20	In progress	In progress		He	
15771	2600-3-4936	704	1300	172	25	1007	35.4	$1.37 \times 10^{-4}$	He	550
15058	2600-3-4936	704	1300	138	20	4045	21.4	$1.72 \times 10^{-5}$	He	2010
15792	2600-3-4936	704	1300	138	20	4588	23.0	$1.08 \times 10^{-5}$	He	1830
16268	2600-3-4936	704	1300	138	20	In progress	In progress		Air	
17328	2600-3-4936	704	1300	103	15	In progress	In progress		He	
16031	2600-3-2792	760	1400	152	22	159.3	57.5	$1.24 \times 10^{-3}$	He	55
16125	2600-3-4936	760	1400	138	20	304.6	38.9	$4.00 \times 10^{-4}$	He	142
17330	2600-3-4936	760	1400	138	20	In progress	In progress		Air	
16490	2600-3-4936	760	1400	103	15	2690	18.7	$1.16 \times 10^{-5}$	He	1480
17332	2600-3-4936	816	1500	69	10	In progress	In progress		He	
16269	2600-3-4936	816	1500	69	10	In progress	In progress		Air	
16054	2600-3-2792	871	1600	62	9	554	34.8	$9.25 \times 10^{-5}$	He	205
16126	2600-3-4936	871	1600	34	5	In progress	In progress		He	

to date or in progress at ORNL in a simulated HTGR helium environment. Table 6 outlines stress-rupture tests planned to be conducted during 1976. Data from five different stress-temperature test conditions generated in air by workers at Cabot-Stellite<sup>18</sup> and data generated in a simulated HTGR environment by workers at General Atomic Co.<sup>19</sup> as well as our own data are given in Table 7. In Fig. 12 all of the stress-rupture data are plotted for comparison purposes. Considering the wide variations known to exist in isothermal stress-rupture data due to subtle differences in heat-to-heat chemistry and variations in product form processing histories, no conclusions can be made regarding the influence of HTGR simulated environments on the stress-rupture properties of Hastelloy X. However, if there are differences they do not appear to be large, at least over the short term. Figure 13 gives the complete creep curves for five ORNL creep tests conducted in helium. Additional data will soon be available from tests in progress.

Table 6. Stress-Rupture Tests to be Conducted on Hastelloy X during 1976.

Heat Number	649°C (1200°F)			704°C (1300°F)		
	Stress		Environment	Stress		Environment
	(MPa)	(ksi)		(MPa)	(ksi)	
2600-3-4936	207	30	He	103	15	Air
2600-3-2792	207	30	He			

#### Fatigue and Creep-Fatigue Interaction

Fully reversed isothermal uniaxial strain-controlled fatigue tests have been completed on a single heat and product form (heat 2600-3-4936, plate) of Hastelloy X over the temperature range from 24 to 871°C (75 to 1600°F). Plots of total strain range,  $\Delta\epsilon_t$ , plastic strain range,  $\Delta\epsilon_p$ , and elastic strain range,  $\Delta\epsilon_e$ , vs cycles to failure are given for room temperature, 538°C (1000°F), 649°C (1200°F), 760°C (1400°F), and 871°C (1600°F) in Figs. 14 to 18 respectively. The data of Jaske and Porfilio<sup>20</sup> were included in the plot of the 760°C (1400°F) data. These tests were conducted at a continuous cycling strain rate of  $4 \times 10^{-3}$ /sec except as noted, using a ramp wave form of the type shown in Fig. 19. Figure 19 also shows wave forms for tests in which a strain dwell or hold period was introduced in either or both the tensile

<sup>20</sup>C. E. Jaske and T. L. Porfilio, *Low-Cycle Fatigue of Type 347 Stainless Steel and Hastelloy X in Hydrogen Gas Environment*, TID/SNA 2047, 1971.

Table 7. Tabulation of Creep and Creep-Rupture Data Obtained from Several Sources and Environments for Hastelloy X

Test No.	Heat No.	Temperature		Stress		Hours for Indicated Creep Strain		Rupture Life (hr)	Elongation (%)	Steady-State Creep Rate ( $10^{-4} \times \text{hr}^{-1}$ )	Environment	Source of Data
		(°C)	(°F)	(MPa)	(ksi)	Creep Strain						
						(2%)	(5%)					
15772	2600-3-4936	649	1200	172	25	850	2170	6466	34.9	0.17	He	ORNL
13167	4248	649	1200	172	25	480	1400			0.32	Air	Cabot
13703	4410	649	1200	172	25	490	1380	7704	68.3	0.28	Air	Cabot
13148	4486	649	1200	172	25	640	1900			0.20	Air	Cabot
12716	94210	649	1200	172	25	950	3200			0.11	Air	Cabot
15058	2600-3-4936	704	1300	138	20	340	1920	4045	21.4	0.17	He	ORNL
15792	2600-3-4936	704	1300	138	20	500	2590	4588	23.0	0.11	He	ORNL
16268	2600-3-4936	704	1300	138	20	300				0.10 <sup>a</sup>	Air	ORNL
	HH2798	760	1400	172	25	3.7	9.9	37.5	84	50	He	GA <sup>b</sup>
	HH2798	760	1400	172	25	4.3	9.3	36.5	86	50	He	GA <sup>b</sup>
13789	4410	760	1400	172	25	4.5	10.0	52.9	91.8	43	Air	Cabot
12552	4438	760	1400	172	25	2.3	5.7	27.0	78.5	85	Air	Cabot
12723	94210	760	1400	172	25	6.0	13.0	54.1	100.9	39	Air	Cabot
16125	2600-3-4936	760	1400	138	20	30	103	304.6	38.9	4.00	He	ORNL
13168	4248	760	1400	138	20	14	36	149.0	68.9	14	Air	Cabot
13788	4410	760	1400	138	20	18	48	513.4	91.5	10	Air	Cabot
12573	4438	760	1400	138	20	8	20	110.1	67.2	25	Air	Cabot
13149	4486	760	1400	138	20	9	33	182.0	86.8	13	Air	Cabot
12593	94210	760	1400	138	20	15	39			13	Air	Cabot
	HH2798	871	1600	69	10	22	67	201.5	79	5.0	He	GA <sup>b</sup>
	HH2798	871	1600	69	10			314	93	3.7	He	GA <sup>b</sup>
13171	4248	871	1600	69	10	9.0	25	70.8	33.6	20	Air	Cabot
13884	4410	871	1600	69	10	6.5	16	76.2	68.9	31	Air	Cabot
12567	4438	871	1600	69	10	4.3	11.6	60.5	45.8	41	Air	Cabot
12564	4438	871	1600	69	10	23.0	69	307.9	41.9	7	Air	Cabot
13152	4486	871	1600	69	10	14.0	40	141.3	39.9	11	Air	Cabot
12588	94210	871	1600	69	10	12.0	38	153.6	53.3	11	Air	Cabot
12571	94210	871	1600	69	10	17.0	54	241.7	63.1	8	Air	Cabot

<sup>a</sup>In the very first step of the steady-state creep and therefore the value is interim.

<sup>b</sup>Data obtained from General Atomic Co.

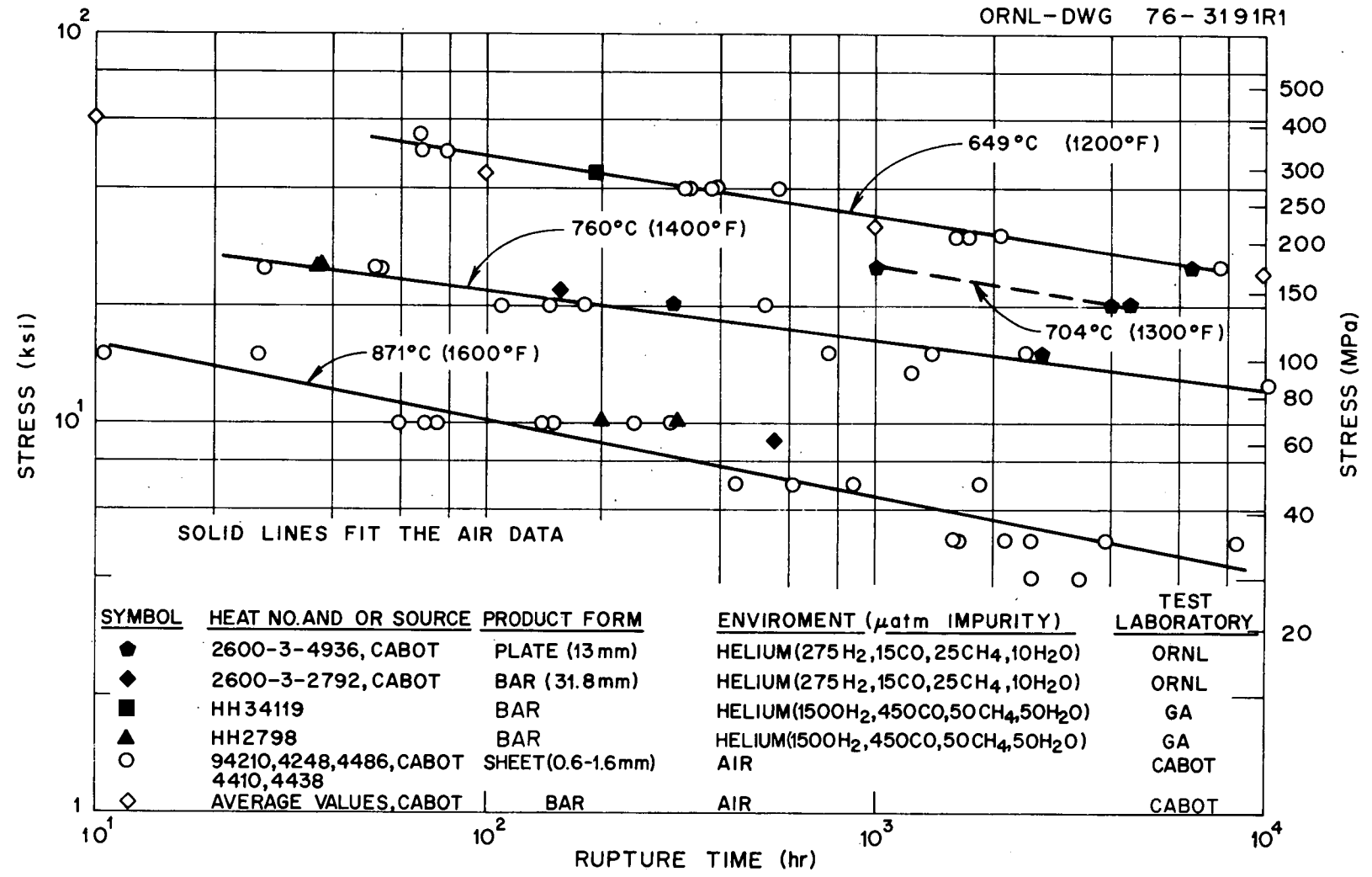


Fig. 12. Isothermal Stress-Rupture Plots for Hastelloy X Comparing Rupture Data from Tests Conducted in Helium with Controlled Impurities ( $1 \text{ atm} = 1.0 \times 10^5 \text{ N/m}^2$ ) and Test Data Generated in Air as Reported From Several Sources.

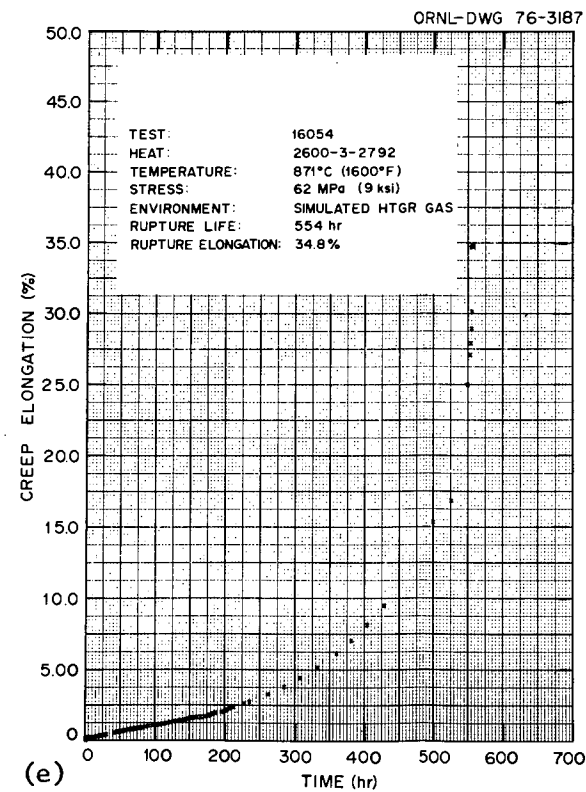
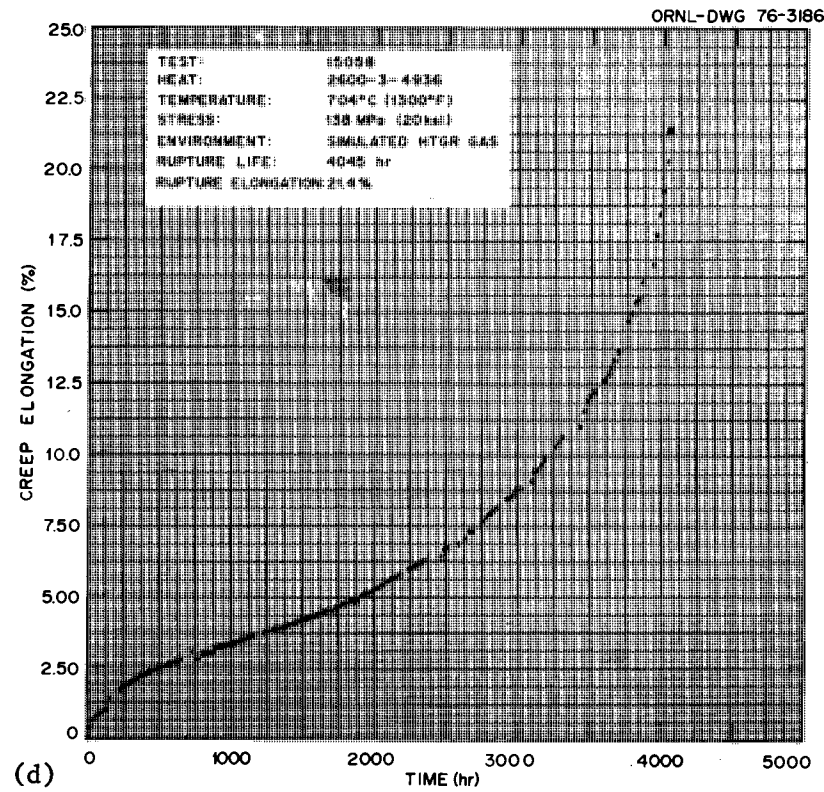
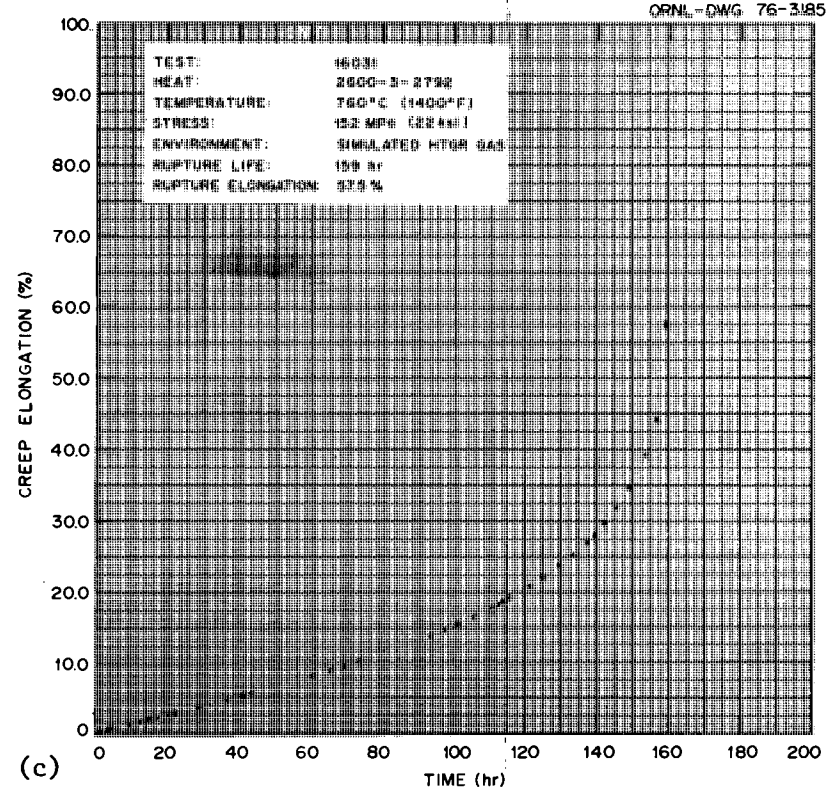
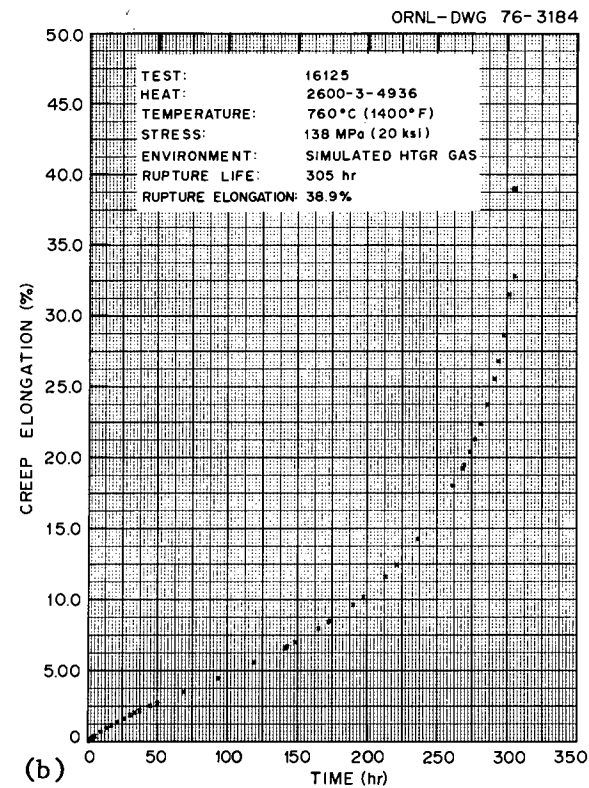
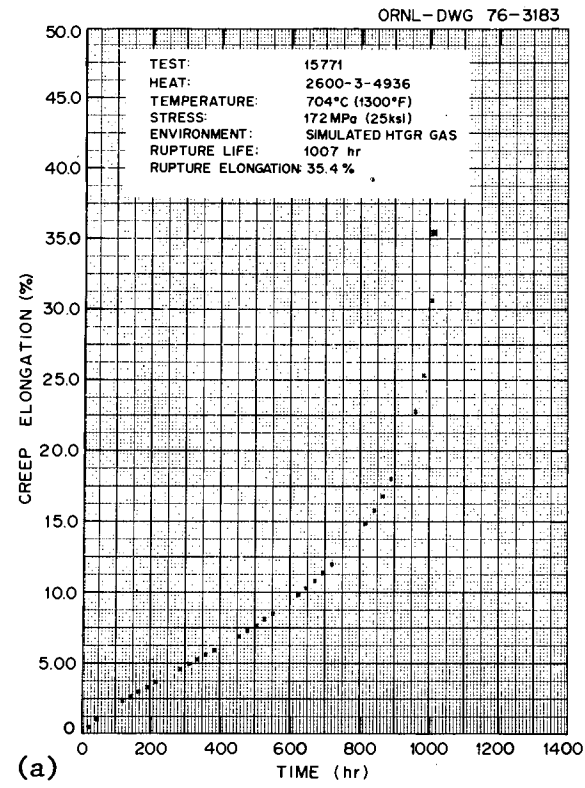


Fig. 13. Creep Elongation as a Function of Time for Hastelloy X.

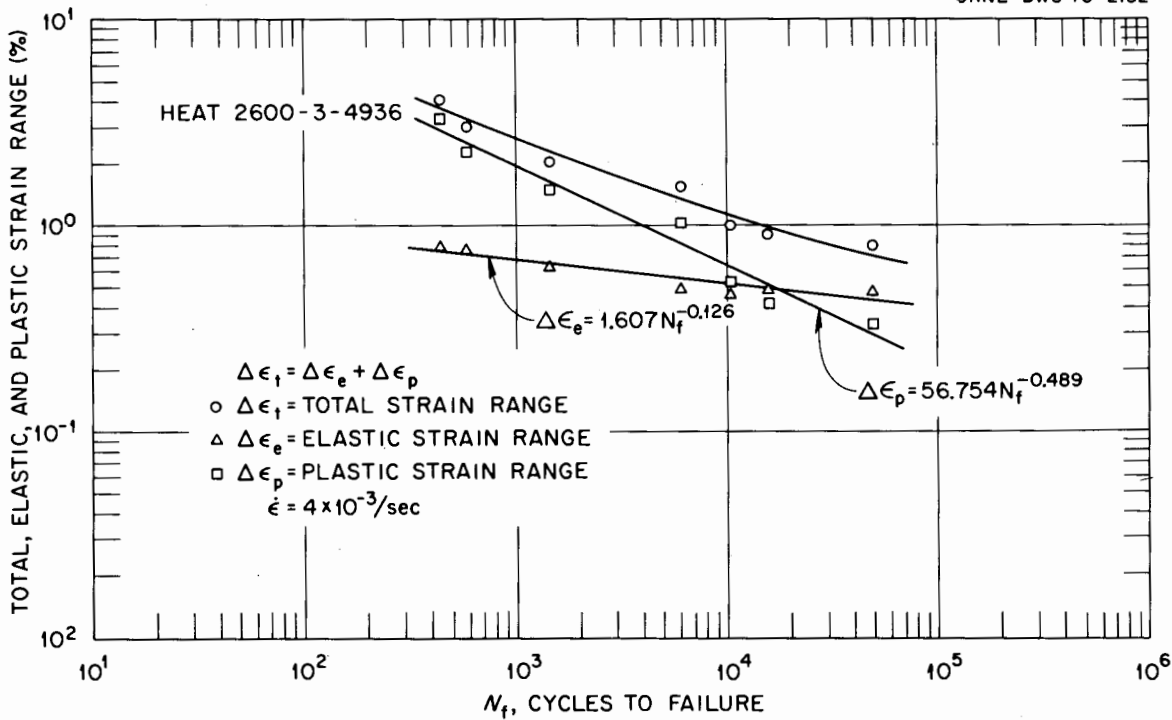


Fig. 14. Total, Elastic, and Plastic Strain Range vs Cycles to Failure at Room Temperature for Hastelloy X Tested in Air.

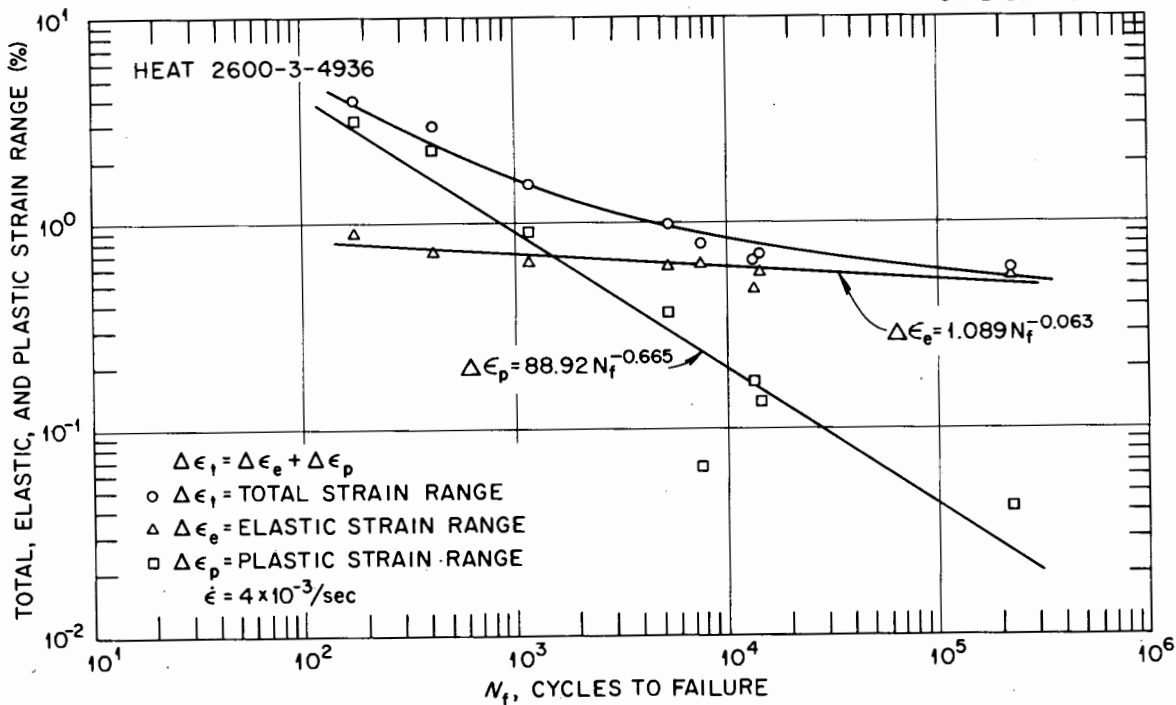


Fig. 15. Total, Elastic, and Plastic Strain Range vs Cycles to Failure at 538°C (1000°F) for Hastelloy X Tested in Air.

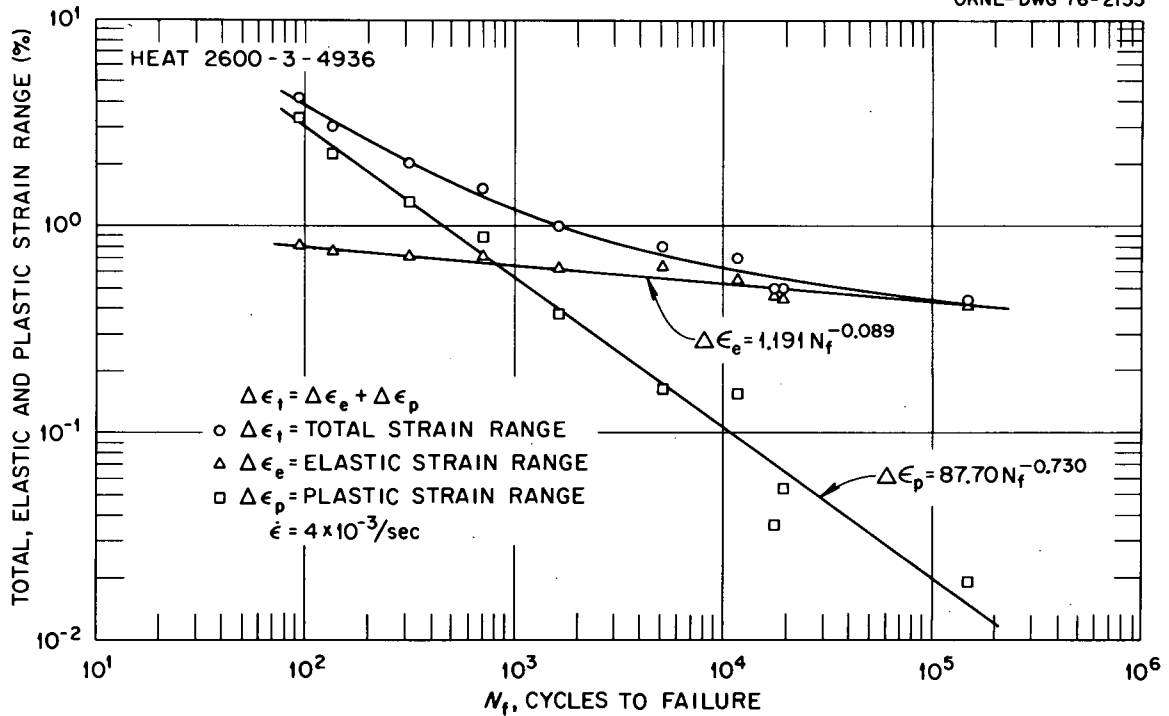


Fig. 16. Total, Elastic, and Plastic Strain Range vs Cycles to Failure at 649°C (1200°F) for Hastelloy X Tested in Air.

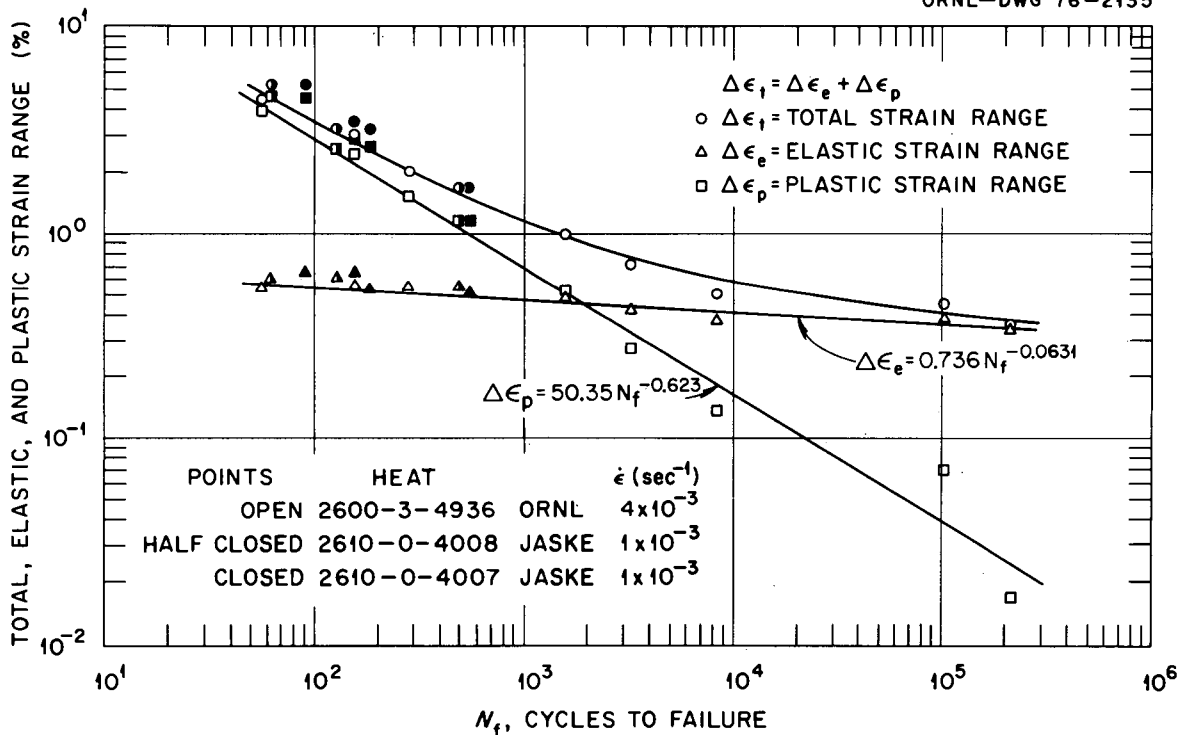


Fig. 17. Total, Elastic, and Plastic Strain Range vs Cycles to Failure at 760°C (1400°F) for Hastelloy X Tested in Air.

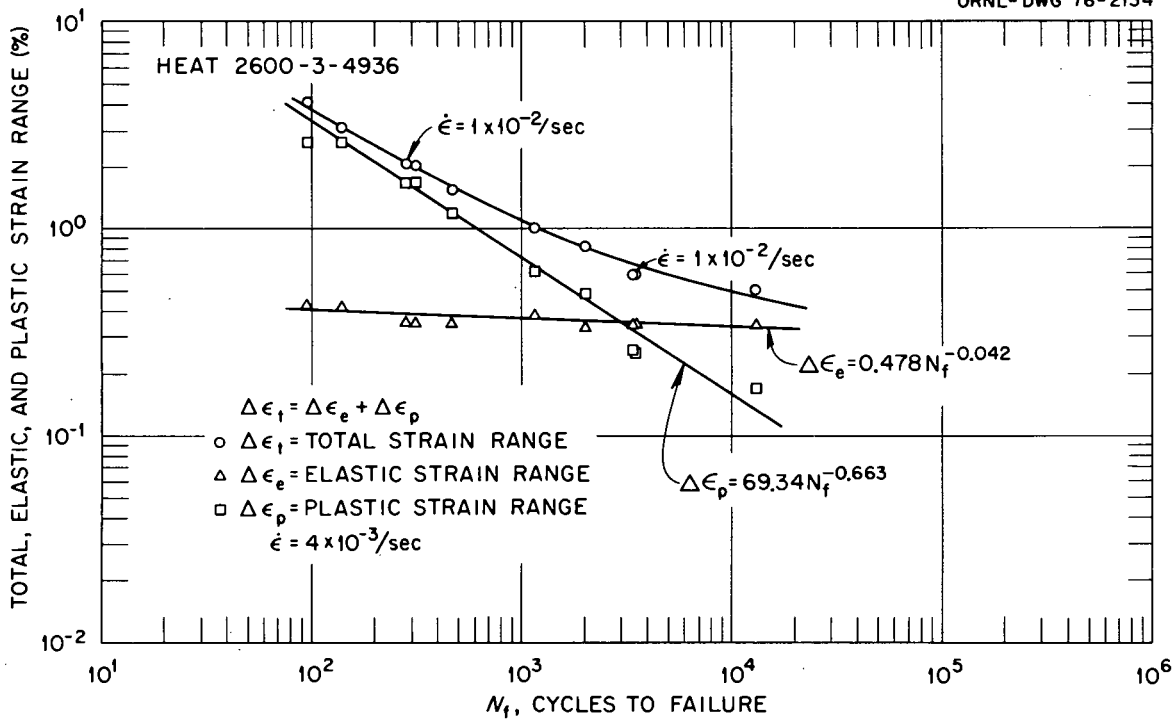


Fig. 18. Total, Elastic, and Plastic Strain Range vs Cycles to Failure at 871°C (1600°F) for Hastelloy X Tested in Air.

and compressive halves of the cycle. Fatigue data generated to date are given in Tables 8 and 9. Figures 14 to 18 demonstrate that the components of the total strain range,  $\Delta \epsilon_t$ , namely the plastic,  $\Delta \epsilon_p$ , and elastic,  $\Delta \epsilon_e$ , strain ranges, can be expressed as simple power law relationships; thus

$$\Delta \epsilon_t = \Delta \epsilon_p + \Delta \epsilon_e, \quad (6)$$

$$\Delta \epsilon_t = AN_f^{-a} + BN_f^{-b}. \quad (7)$$

Values of the coefficients and exponents in the above equation have been determined by linear least-squares analysis and are summarized in Table 10.

In Fig. 20 a summary comparison best-fit plot is given of the isothermal total strain range vs cycles to failure data. Increasing the temperature generally decreases the continuous-cycling fatigue life of Hastelloy X as shown. Several tests were conducted at a strain rate of  $1 \times 10^{-2}/\text{sec}$  at 871°C (1600°F) in order to determine if fatigue life was strain-rate dependent within the creep range at strain rates in excess of  $4 \times 10^{-3}/\text{sec}$ . The results of the higher strain rate tests gave essentially identical cyclic lives, indicating strain-rate independence for strain rates equal to or in excess of  $4 \times 10^{-3}/\text{sec}$ .

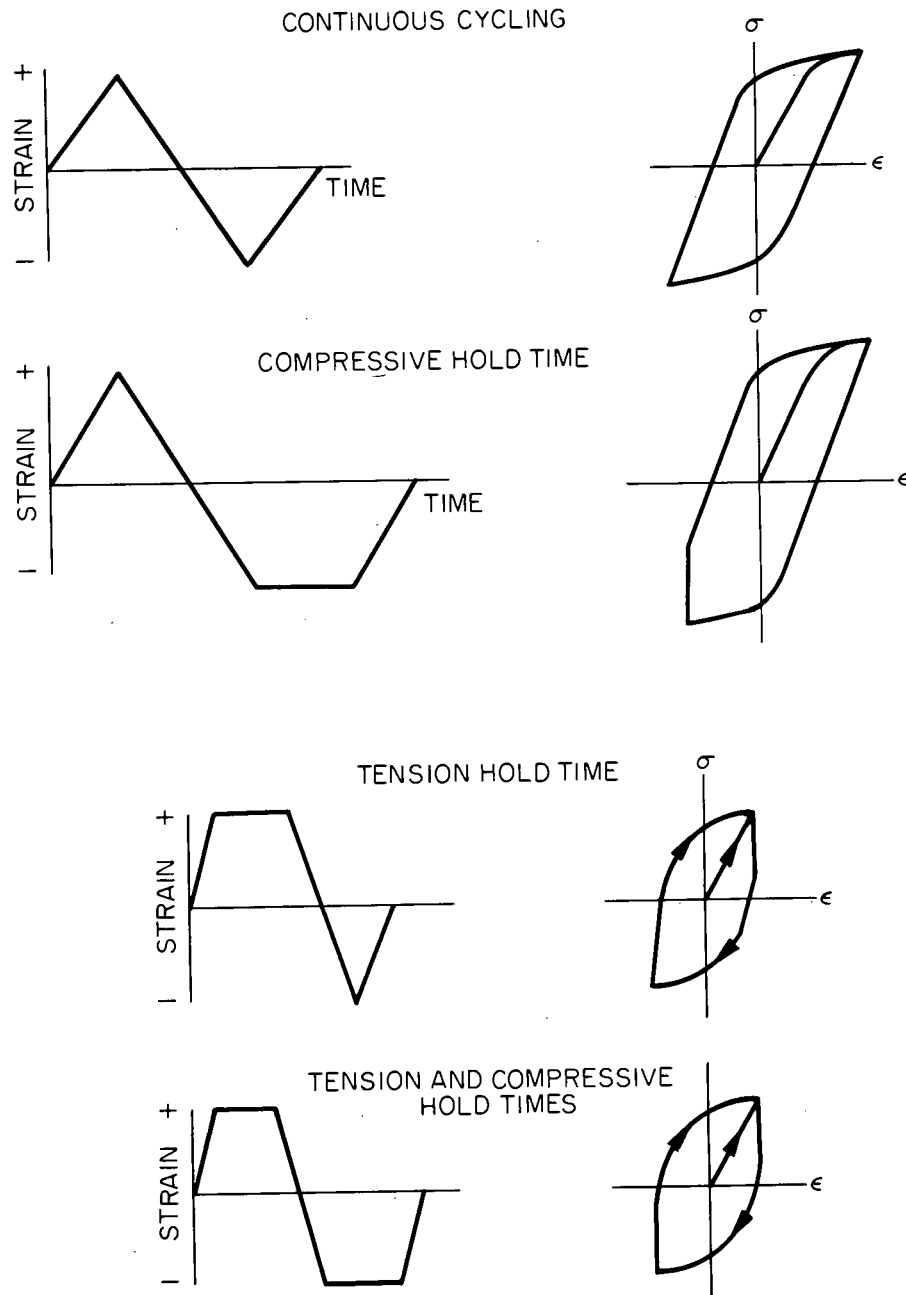


Fig. 19. Strain-Time Wave Forms and Associated Stress-Strain Hysteresis Loops for Fatigue and Creep-Fatigue Tests.

Table 8. Results of Strain-Controlled Fatigue Tests on Hastelloy X  
[Heat 2600-3-4936 13-mm (1/2 in.) Plate] Tested in Air<sup>a</sup>

Specimen <sup>b</sup>	Poisson's Ratio, $\nu$	Total Strain Range, $\Delta\epsilon_t$	Strain Range at $N_f/2$ , $\epsilon$				Cycles to Failure, $N_f$	Time to Failure, $t_f$	Stress Range at 10th Cycle, $\Delta\sigma_{10}$		Properties of $N_f/2$ , MPa (ksi)		
			Elastic, $\Delta\epsilon_e$		Inelastic, $\Delta\epsilon_{in}$				MPa	(ksi)	Stress Range <sup>c</sup>	Tensile Stress Amplitude, $\sigma_T$	Compressive Stress Amplitude, $\sigma_C$
			Measured	Calculated <sup>c</sup>	Measured	Calculated <sup>d</sup>							
Tested at 22°C (72°F) (Young's Modulus $E = 199 \text{ GPa} = 28.87 \times 10^6 \text{ psi}$ )													
HXL-51	0.315	4.10	0.79	0.72	3.31	3.38	439	146	1292	187.4	1425 (206.7)	698 (101.3)	727 (105.4)
HXL-29	0.265	3.04	0.76	0.70	2.28	2.34	591	148	1237	179.5	1392 (201.9)	681 (98.8)	711 (103.1)
HXL-28	0.285	2.11	0.62	0.59	1.49	1.51	1,494	249	1087	157.7	1177 (170.8)	584 (84.8)	593 (86.0)
HXL-27	0.280	1.50	0.49	0.49	1.02	1.02	6,101	763	956	138.6	968 (140.4)	478 (69.3)	490 (71.1)
HXL-23	0.278	0.99	0.46	0.43	0.53	0.56	10,245	854			862 (125.0)	427 (62.0)	435 (63.1)
HXL-47	0.261	0.89	0.48	0.42	0.41	0.47	15,796	1,185	815	118.1	829 (120.3)	407 (59.1)	422 (61.2)
HXL-22	0.269	0.80	0.46	0.42	0.33	0.38	49,664	3,311			837 (121.4)	406 (58.9)	431 (62.5)
Tested at 538°C (1000°F) (Young's Modulus $E = 162 \text{ GPa} = 23.54 \times 10^6 \text{ psi}$ )													
HXL-46	0.299	4.06	0.89	0.94	3.18	3.12	177	59	1084	157.2	1530 (221.9)	748 (108.4)	782 (113.5)
HXL-16	0.306	3.02	0.73	0.83	2.94	2.19	418	104	847	122.8	1353 (196.3)	665 (96.5)	688 (99.8)
HXL-20	0.274	1.56	0.65	0.70	0.91	0.86	1,181	148	764	110.8	1141 (165.5)	562 (81.6)	579 (83.9)
HXL-30	0.302	0.99	0.62	0.63	0.37	0.36	5,182	432	666	96.6	1015 (147.3)	494 (71.7)	521 (75.6)
HXL-3	0.268	0.79	0.73	0.67	0.06	0.12	7,596	501			1084 (157.2)	493 (71.5)	591 (85.8)
HXT-2	0.290	0.71	0.57	0.53	0.13	0.18	14,240	831	577	83.7	855 (124.0)	405 (58.7)	450 (65.3)
HXT-4	0.320	0.65	0.48	0.56	0.17	0.08	13,675	741	542	78.6	917 (133.0)	446 (64.7)	471 (68.3)
HXL-19	0.341	0.60	0.56	0.54	0.04	0.06	225,000	11,250			877 (127.2)	444 (64.4)	433 (62.8)
Tested at 649°C (1200°F) (Young's Modulus $E = 154 \text{ GPa} = 22.4 \times 10^6 \text{ psi}$ )													
HXL-6	0.312	4.17	0.80	0.96	3.37	3.21	94	31	1118	162.3	1476 (214.0)	719 (104.2)	757 (109.8)
HXL-14	0.323	3.00	0.76	0.91	2.24	2.09	133	33	1059	153.6	1412 (204.8)	693 (100.6)	719 (104.2)
HXL-42	0.316	2.03	0.72	0.82	1.31	1.21	318	53	872	126.5	1258 (182.5)	611 (88.6)	647 (93.8)
HXL-44	0.334	1.52	0.63	0.72	0.89	0.80	713	89	711	103.1	1119 (162.3)	547 (79.3)	572 (83.0)
HXL-8	0.305	1.00	0.63	0.63	0.38	0.37	1,617	135			972 (141.0)	478 (69.3)	494 (71.7)
HXT-3	0.270	0.80	0.64	0.59	0.16	0.22	5,147	343	628	91.1	909 (131.8)	438 (63.5)	471 (68.3)
HXL-10	0.308	0.70	0.55	0.54	0.15	0.16	11,764	686			831 (120.5)	406 (58.9)	425 (61.6)
HXL-7	0.325	0.50	0.45	0.47	0.05	0.03	19,262	802			731 (106.2)	371 (53.9)	360 (52.3)
HXL-1	0.258	0.50	0.46	0.46	0.04	0.04	17,820	742			715 (103.8)	382 (55.5)	333 (48.3)
HXL-15	0.381	0.44	0.42	0.45	0.02	0.03	148,497	5,445	454	65.9	700 (101.6)	351 (51.0)	349 (50.6)
Tested at 760°C (1400°F) (Young's Modulus $E = 146 \text{ GPa} = 21.16 \times 10^6 \text{ psi}$ )													
HXL-13	0.321	4.48	0.54	0.70	3.94	3.78	56	21	966	140.1	1016 (147.4)	494 (71.7)	522 (75.7)
HXL-11	0.305	3.00	0.55	0.64	2.45	2.36	154	38	848	123.0	935 (135.7)	465 (67.4)	470 (68.2)
HXL-48	0.282	2.07	0.55	0.62	1.52	1.45	280	46	725	105.2	902 (130.8)	449 (65.2)	453 (65.6)
HXL-50	0.316	1.50	0.50	0.55	1.00	0.95	598	75	663	96.2	800 (116.1)	396 (57.4)	404 (58.7)
HXL-2	0.294	1.0	0.48	0.47	0.52	0.53	1,582	132			684 (99.2)	339 (49.2)	345 (50.0)
HXL-17	0.320	0.70	0.42	0.45	0.28	0.25	3,351	195			655 (95.0)	323 (46.9)	332 (48.1)
HXL-18	0.369	0.51	0.37	0.40	0.14	0.11	8,362	348	434	63.0	586 (85.0)	293 (42.5)	293 (42.5)
HXT-5	0.267	0.45	0.38	0.35	0.07	0.10	102,168	3,831	460	66.7	518 (75.1)	256 (37.2)	262 (38.0)
HXL-5	0.308	0.35	0.34	0.32	0.02	0.03	215,747	6,293	363	52.7	476 (69.0)	213 (30.9)	263 (38.1)
Tested at 871°C (1600°F) (Young's Modulus $E = 137 \text{ GPa} = 19.86 \times 10^6 \text{ psi}$ )													
HXL-41	0.311	4.00	0.42	0.53	3.58	3.47	96	32	702	101.8	720 (104.7)	347 (50.4)	373 (54.0)
HXL-40	0.326	3.01	0.41	0.52	2.60	2.49	138	34	690	100.1	715 (103.7)	343 (49.7)	372 (54.0)
HXL-33	0.337	2.01	0.34	0.44	1.67	1.57	312	52	536	77.8	610 (88.5)	298 (43.2)	312 (45.3)
HXL-53 <sup>e</sup>	0.319	2.00	0.35	0.44	1.65	1.56	280	19	609	88.4	682 (99.0)	333 (48.3)	349 (50.7)
HXL-34 <sup>f</sup>	0.298	2.00	0.47	0.47	1.53	1.53	216	1,332	566	82.0	638 (92.6)	318 (46.1)	320 (46.4)
HXL-35 <sup>g</sup>	0.329	2.00	0.48	0.48	1.52	1.48	185	1,141	536	77.7	655 (95.0)	333 (48.2)	322 (46.8)
HXL-37 <sup>g,h</sup>	0.320	2.00	0.47	0.47	1.53	1.53	196	2,384	521	75.6	644 (93.4)	319 (46.3)	325 (47.1)
HXT-7	0.307	1.50	0.34	0.44	1.16	1.06	466	58	542	78.6	604 (87.5)	297 (43.1)	307 (44.5)
HXL-36	0.305	1.00	0.38	0.38	0.62	0.62	1,156	96	486	70.4	523 (75.8)	257 (37.2)	266 (38.6)
HXL-54 <sup>h</sup>	0.274	0.99	0.389	0.389	0.601	0.601	618	9,322	417	60.5	533 (77.3)	275 (39.8)	258 (37.4)
HXL-43	0.307	0.80	0.32	0.35	0.48	0.45	2,002	133			479 (69.5)	236 (34.2)	243 (35.2)
HXL-21	0.270	0.59	0.34	0.33	0.25	0.26	3,433	172	408	59.2	452 (65.6)	229 (33.2)	223 (32.4)
HXL-24 <sup>e</sup>	0.279	0.59	0.34	0.34	0.25	0.25	3,494	70			460 (66.8)	232 (33.6)	228 (33.2)
HXL-26 <sup>f,i</sup>	0.253	0.60	0.37	0.37	0.23	0.23	2,191	13,255	385	55.8	509 (73.8)	219 (31.8)	290 (42.1)
HXL-32 <sup>g,i</sup>	0.315	0.60	0.37	0.37	0.23	0.23	1,084	6,558	383	55.5	510 (74.1)	274 (39.8)	236 (34.3)
HXL-38 <sup>f,g</sup>	0.283	0.60	0.36	0.36	0.24	0.24	984	11,857	394	57.2	495 (71.8)	247 (35.9)	248 (35.9)
HXT-6	0.255	0.50	0.34	0.28	0.16	0.22	13,234	551	374	54.3	392 (56.9)	195 (28.3)	197 (28.6)

<sup>a</sup>Strain rate  $4 \times 10^{-3}$ /sec unless otherwise noted.

<sup>b</sup>L in specimen number implies specimen axis parallel to rolling direction; T transverse.

<sup>c</sup> $\Delta\sigma/E$ .

<sup>d</sup> $\Delta\epsilon_e - \Delta\sigma/E$ .

<sup>e</sup>Strain rate  $10 \times 10^{-3}$ /sec.

<sup>f</sup>0.1-hr tensile hold period.

<sup>g</sup>0.1-hr compressive hold period.

<sup>h</sup>0.25-hr compressive hold period.

<sup>i</sup>Strain rate  $9 \times 10^{-3}$ /sec.

Table 9. Strain-Range Partitioning in Strain-Controlled Fatigue Tests on Hastelloy X in Air at 871°C (1600°F)

Specimen	Strain Rate (sec <sup>-1</sup> )	Hold Period, hr		Relaxed Stress, MPa (ksi)		Partitioned Inelastic Strain Range, <sup>a</sup> %		Associated Cycle Lifetimes, hr	
		Tensile	Compressive	Tensile, $\sigma_t$	Compressive, $\sigma_c$	$\Delta\epsilon_{pp}$	Other	$N_{pp}$	Other
HXL-34	$4 \times 10^{-3}$	0.1		48 (7.0)		1.34	$\Delta\epsilon_{cp} = 0.20$	312	$N_{cp} = 70$
HXL-35	4		0.1		38 (5.6)	1.31	$\Delta\epsilon_{pc} = 0.21$	320	$N_{pc} = 50$
HXL-37	4	0.1	0.1	33 (4.8)	33 (4.8)	1.32	$\Delta\epsilon_{cc} = 0.21$	318	$N_{cc} = 58$
HXL-54	4		0.25		38 (5.6)	0.44	$\Delta\epsilon_{pc} = 0.16$	1,746	$N_{pc} = 222$
HXL-26	9	0.1		57 (8.3)		0.11	$\Delta\epsilon_{cp} = 0.11$	15,039	$N_{cp} = 1221$
HXL-32	9		0.1		49 (7.1)	0.090	$\Delta\epsilon_{pc} = 0.14$	20,604	$N_{pc} = 669$
HXL-38	4	0.1	0.1	26 (3.9)	30 (4.3)	0.079	$\Delta\epsilon_{cc} = 0.16$	25,228	$N_{cc} = 667$

<sup>a</sup>Based on calculated inelastic strain range.

Table 10. Values for the Elastic and Plastic Strain Range Constants for Strain-Controlled Tests Conducted on Hastelloy X at a Strain Rate of  $4 \times 10^{-3}$ /sec

Heat	Temperature		Values of Constants in $\Delta\epsilon_t = AN_f^{-a} + BN_f^{-b}$			
	(°C)	(°F)	A	a	B	b
	2600-3-4936	Room	Room	56.75	0.489	1.607
2600-3-4936	538	1000	88.92	0.665	1.089	0.0633
2600-3-4936	649	1200	87.70	0.730	1.191	0.0890
2600-3-4936	700	1400	50.35	0.623	0.736	0.0631
2600-3-4936	871	1600	69.34	0.663	0.478	0.0420

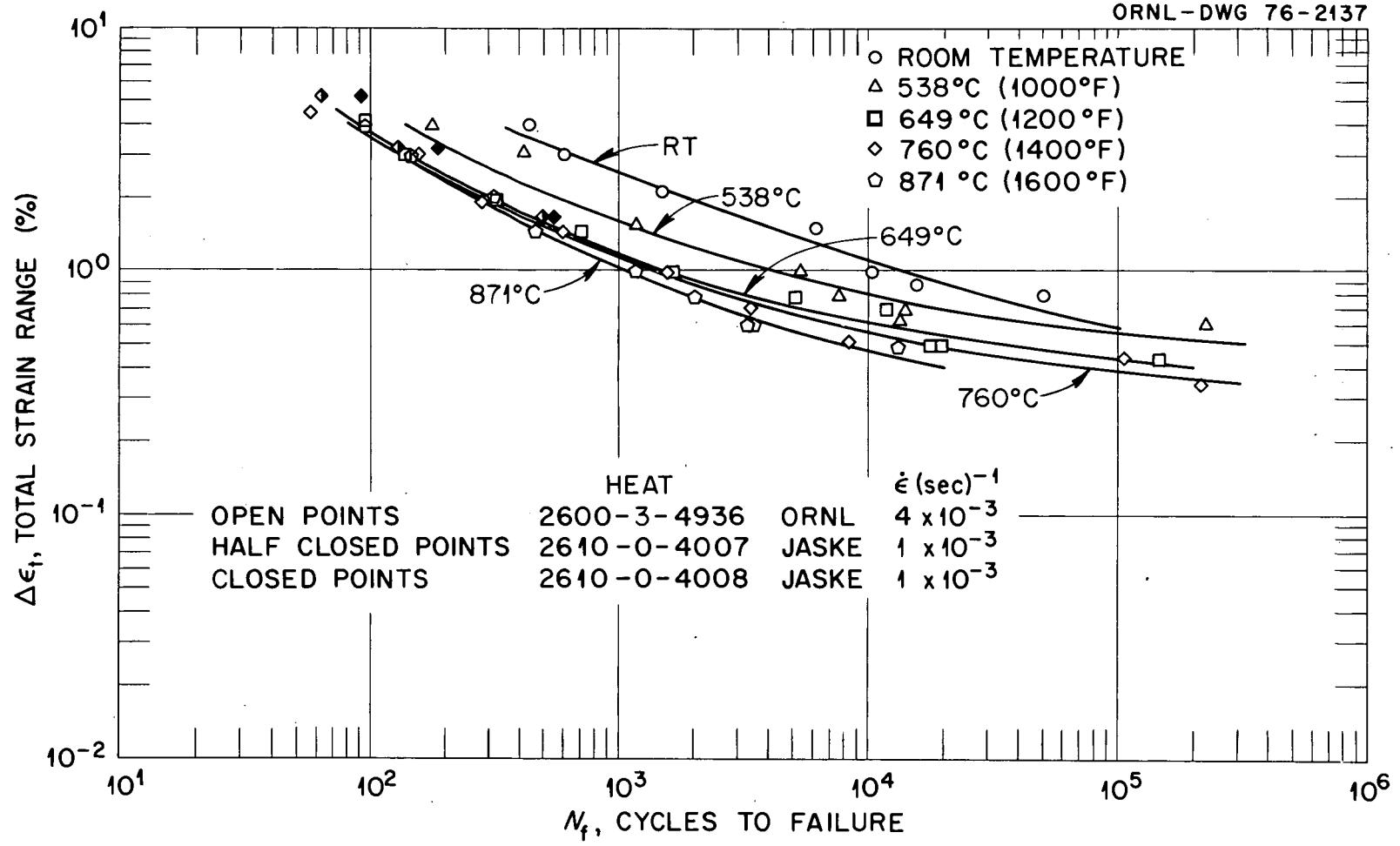


Fig. 20. Total Strain Range vs Cycles to Failure for Hastelloy X Tested in Air.

Since other structural materials<sup>21,22</sup> will be used for various components within HTGR systems, it was thought instructive to make comparisons between the continuous-cycling fatigue properties of Hastelloy X and a number of these materials. These materials include Inconel alloy 718,<sup>23</sup> Incoloy alloy 800,<sup>24-27</sup> 2 1/4 Cr-1 Mo steel,<sup>28</sup> type 304 stainless steel,<sup>24-27,29,30</sup> type 316 stainless steel,<sup>24,26,31</sup> and AISI 1010 steel.<sup>32</sup> Product forms from which the data were generated, along with several tensile properties of interest in fatigue analysis at temperatures where comparisons can be made, are given in Table 11. All data were generated in air at a continuous-cycling strain rate of  $4 \times 10^{-3}$ /sec. Comparative plots are given in Figs. 21-23. Values of

---

<sup>21</sup>P. L. Rittenhouse, *Initial Assessment of the Status of HTGR Metallic Structural Materials Technology*, ORNL-TM-4760 (December 1974).

<sup>22</sup>P. L. Rittenhouse and C. S. Morgan, *Status Report on Structural Materials of HTGR Primary System Components*, ORNL/TM-5136 (January 1976).

<sup>23</sup>C. R. Brinkman and G. E. Korth, "Strain Fatigue and Tensile Behavior of Inconel 718 from Room Temperature to 650°C," *J. Test. Eval.* 2(4): 249-59 (July 1974).

<sup>24</sup>J. B. Conway, R. H. Stentz, and J. T. Berling, *Fatigue, Tensile and Relaxation Behavior of Stainless Steels*, USAEC TID-26135, Division of Reactor Research and Development, U.S. Atomic Energy Commission (1975).

<sup>25</sup>D. L. Keller, *Progress on LMFBR Cladding, Structural, and Component Material Studies During July 1971 Through June 1972 - Final Report Task 32*, BMI-1928, Battelle Columbus Laboratories.

<sup>26</sup>D. L. Keller, *Progress on LMFBR Cladding, Structural, and Component Materials Studies During July 1970 Through June 1971 - Annual Report, Task 32, Final Report, Task 14*, BMI-1914, Battelle Columbus Laboratories.

<sup>27</sup>Component and Systems Development Program, *Quart. Prog. Rep. June 30, 1975*, GA-A13512, General Atomic Company.

<sup>28</sup>C. R. Brinkman et al., *Interim Report on the Continuous Cycling Elevated-Temperature Fatigue and Subcritical Crack Growth Behavior of 2 1/4 Cr-1 Mo Steel*, ORNL-TM-4993 (December 1975).

<sup>29</sup>Personal communication with D. R. Diercks, January 1976.

<sup>30</sup>C. R. Brinkman and G. E. Korth, *Heat-to-Heat Variations in the Fatigue and Creep-Fatigue Behavior of AISI Type 304 Stainless Steel, and the Fatigue Behavior of Type 308 Stainless Steel Weld Materials*, ANCR-1097 Aerojet Nuclear Company (May 1973).

<sup>31</sup>C. R. Brinkman, G. E. Korth, and R. R. Hobbins, "Estimates of Creep-Fatigue Interaction in Irradiated and Unirradiated Austenitic Stainless Steels," *Nucl. Technol.* 16: 297-307 (October 1972).

<sup>32</sup>C. E. Jaske, "Low Cycle Fatigue of AISI 1010 Steel at Temperatures up to 1200°F (649°C)," to be presented at American Society of Mechanical Engineers International Joint Pressure Vessels and Piping and Petroleum Mechanical Engineering Conference, September 19-24, 1976, Mexico City, Mexico.

Table 11. Comparison of Several Tensile Properties  
(average values) of Several Structural Materials  
Used in Nuclear Reactor Construction

Material and Heat Treatment	20°C (70°F)	538°C (1000°F)	649°C (1200°F)
<u>Inconel Alloy 718</u> (Plate), Solution Annealed at 954°C (1750°F); Duplex Aged at 718/621°C (1325/1150°F)			
Ultimate Tensile Strength, MPa (ksi)	1372 (199)	1193 (173)	1069 (155)
Yield Strength, MPa (ksi)	1034 (150)	965 (140)	903 (131)
Reduction of Area (%)	28	27	23
<u>Hastelloy Alloy X</u> (Plate), Solution Annealed at 1176°C (2150°F) followed by rapid air cool or water quench			
Ultimate Tensile Strength, MPa (ksi)	758 (110)	593 (86)	510 (74)
Yield Strength, MPa (ksi)	358 (52)	227 (33)	221 (32)
Reduction of Area (%)	60	38	38
<u>Incoloy Alloy 800, Grades 2</u> (Bar), and H, Solution Annealed at 1148°C (2100°F)			
Ultimate Tensile Strength, MPa (ksi)	545 (79)	448 (65)	379 (55)
Yield Strength, MPa (ksi)	228 (33)	131 (19)	117 (17)
Reduction of Area (%)	73	55	53
<u>Type 316 Stainless Steel</u> (Bar), Solution Annealed			
Ultimate Tensile Strength, MPa (ksi)	593 (86)	455 (66)	365 (53)
Yield Strength, MPa (ksi)	250 (37)	172 (25)	165 (24)
Reduction of Area (%)	72	66	69
<u>Type 304 Stainless Steel</u> (Bar), Solution Annealed			
Ultimate Tensile Strength, MPa (ksi)	593 (86)	393 (57)	290 (42)
Yield Strength, MPa (ksi)	248 (36)	131 (19)	117 (17)
Reduction of Area (%)	81	69	58
<u>2 1/4 Cr-1 Mo Steel</u> , Plate and Pipe, Annealed or Isothermally Annealed			
Ultimate Tensile Strength, MPa (ksi)	500 (73)	380 (55)	
Yield Strength, MPa (ksi)	260 (37)	195 (28)	
Reduction of Area (%)	70	75	
<u>AISI 1010 Steel</u> , Hot-Rolled 3/4-in.-diam (1.91-cm) bar			
Ultimate Tensile Strength, MPa (ksi)	369 (54)	153 (22)	
Yield Strength, MPa (ksi)	261 (38)	92 (13)	
Reduction of Area (%)	74	90	

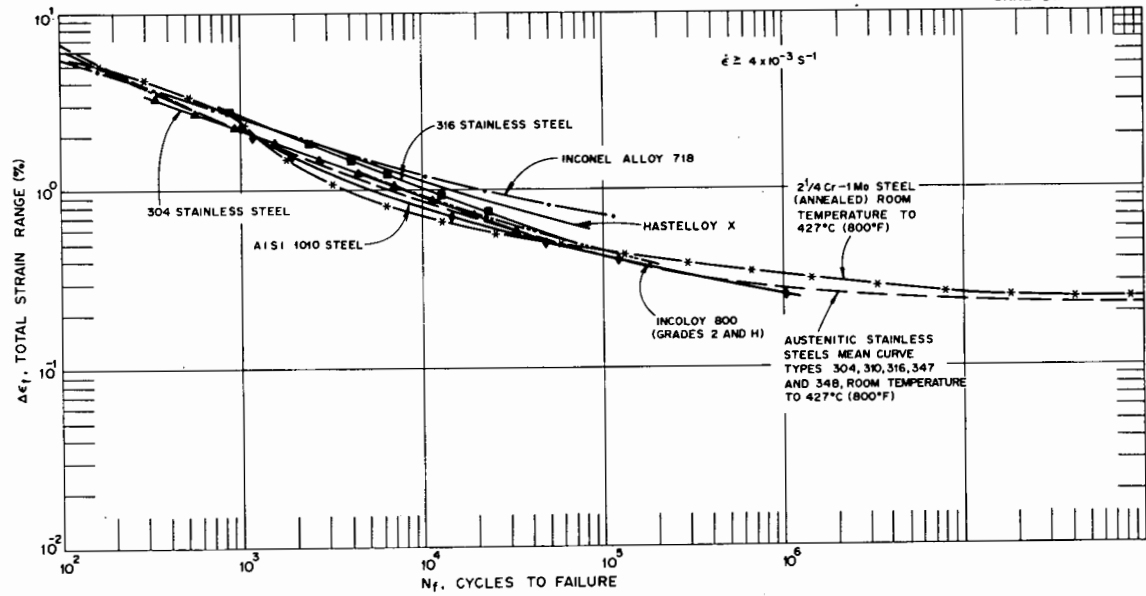


Fig. 21. Comparison of the Fatigue Behavior of Several Materials at Room Temperature (Except as Indicated). Lines represent best-fit values of actual data.

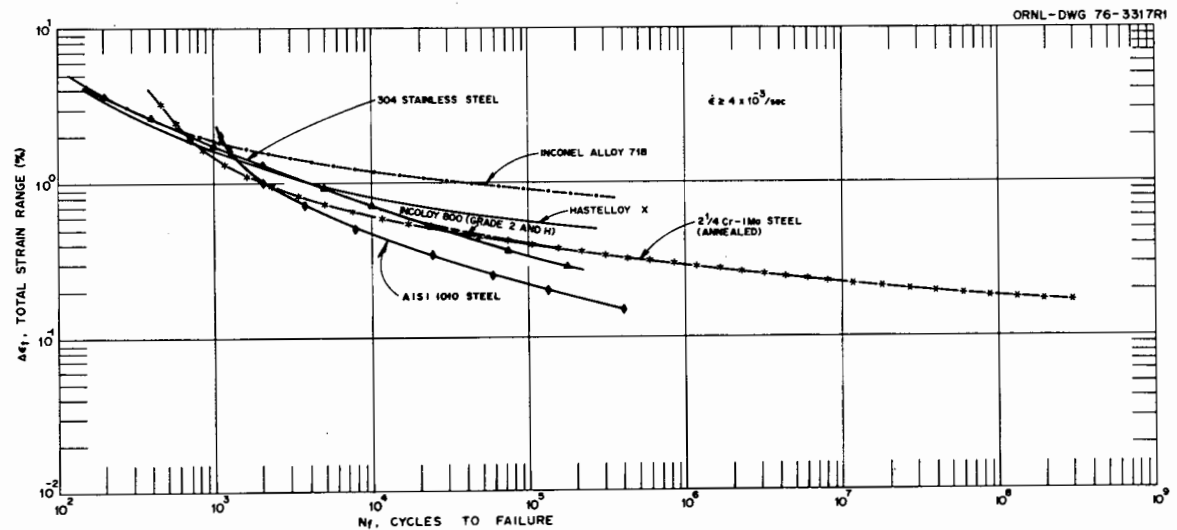


Fig. 22. Comparison of the Fatigue Behavior of Several Materials at 538°C (1000°F). Lines represent best-fit values of actual data. Data for type 304 stainless steel include tests conducted at 538°C (1000°F) and 566°C (1050°F).

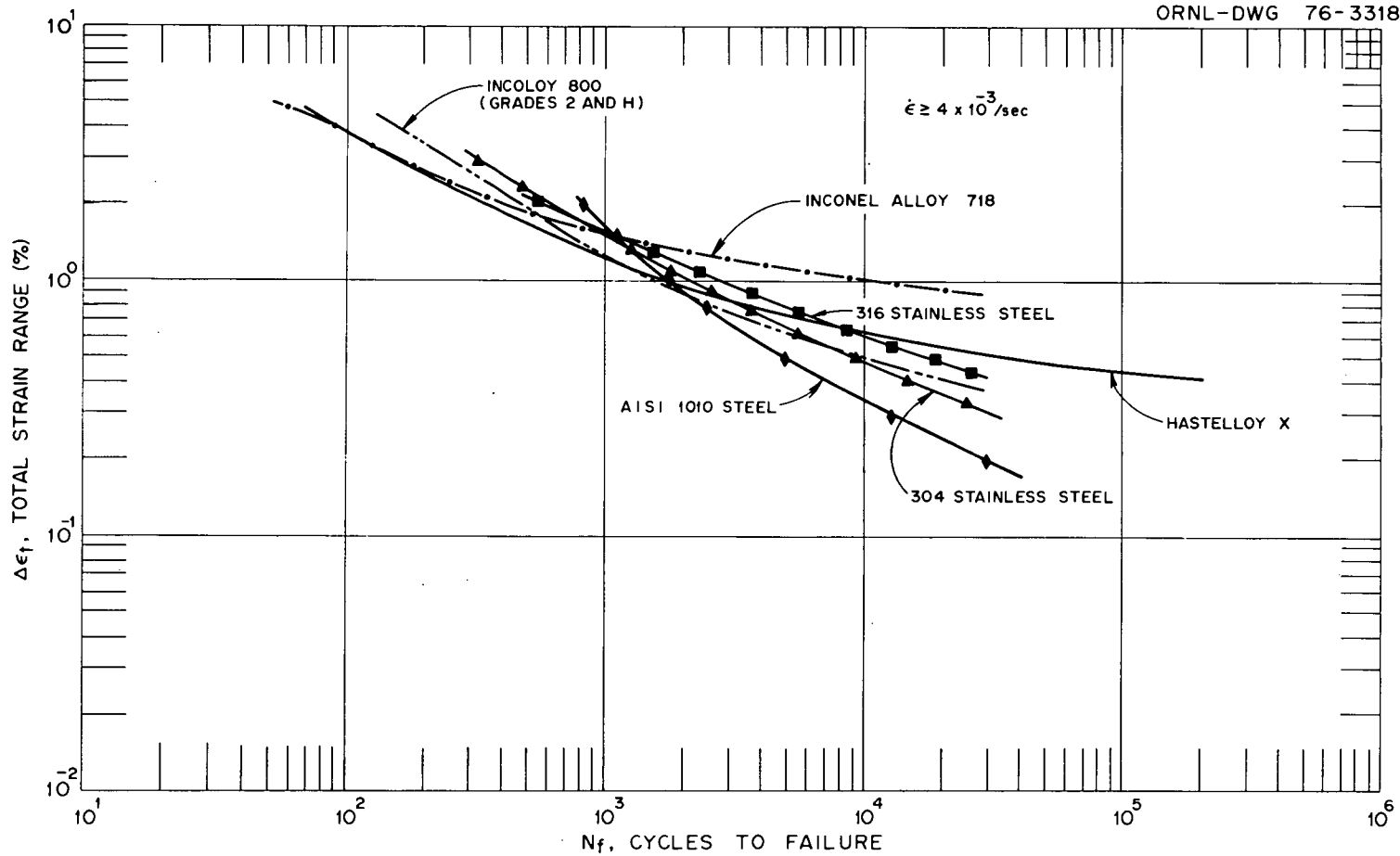


Fig. 23. Comparison of the Fatigue Behavior of Several Materials at 649°C (1200°F). Lines represent best-fit values of actual data.

the constants defining equations for Hastelloy X are given in Table 10, while equations for other materials are given in the Appendix.

Comparing the continuous-cycling fatigue of these materials in Figs. 21-23 indicates similar low-cycle fatigue behavior in the low-cycle range, even though they show wide differences in ductility, particularly at room temperature. However, as the total strain range is reduced, marked differences in fatigue life occur which are accentuated by increasing the temperature. High-cycle fatigue resistance is a function of the ultimate tensile strength, and, therefore, Inconel alloy 718, having the highest value, shows the best high-cycle fatigue resistance, with Hastelloy X showing the second best.

In addition to continuous-cycling fatigue tests, hold periods at constant strain (see Fig. 19) and load are being introduced each cycle in order to determine the influence of creep-fatigue and environmental interaction on the flow and failure behavior of Hastelloy X. Generally, the technique of strain range partitioning<sup>33,34</sup> is being used as a guide in developing the necessary data. The experimental steps in order to generate the data so that the fatigue life of any complex cycle at temperatures within the creep range might be predicted are as follows:

1. generate curves for various inelastic strain modes, that is,  $\Delta\epsilon_{pp}$ ,  $\Delta\epsilon_{cp}$ ,  $\Delta\epsilon_{pc}$ , and  $\Delta\epsilon_{cc}$ ;
2. conduct tests with mixed strain modes (two) to verify position of lines (single temperature);
3. conduct tests at several temperatures, including peak expected operating temperature (normal or accident) to verify damage lines;
4. conduct complex hysteresis loop tests;
5. conduct long-term tests for verification;
6. conduct environmental tests to determine impact of particular environments;

where

$\Delta\epsilon_{pp}$  = range of tensile plasticity reversed by compressive plasticity strain or width of the hysteresis loop generated at high enough strain rates to preclude creep or strain-rate effects; in Hastelloy X over the temperature range of interest, strain rates equal to or in excess of  $4 \times 10^{-3}$ /sec were shown to be acceptable for this purpose;

---

<sup>33</sup>S. S. Manson, G. R. Halford, and M. H. Firshberg, "Creep-Fatigue Analysis by Strain-Range Partitioning," pp. 12-28 in *Symposium on Design for Elevated Temperature Environments*, ed. by S. Y. Zamrik, American Society of Mechanical Engineers, New York, 1971.

<sup>34</sup>M. H. Hirshberg and G. R. Halford, "Use of Strain-Range Partitioning to Predict High-Temperature Low-Cycle Fatigue Life," NASA Lewis Research Center, Cleveland, Ohio (to be published).

- $\Delta\epsilon_{cp}$  = range of tensile creep reversed by compressive plasticity strain generated in work to date by tensile strain hold-time tests; however, other tests imposing load holds will also be conducted;
- $\Delta\epsilon_{pc}$  = range of tensile plasticity strain reversed by compressive creep strain; obtained from compressive hold-time tests; to date, only strain hold-time tests have been conducted;
- $\Delta\epsilon_{cc}$  = range of tensile creep reversed by compressive creep; obtained from tests in which a hold is introduced during both the tensile and compressive halves of each cycle; only strain holds have been conducted to date.

At this time, only a limited number of hold-time tests, all in the strain-controlled mode, have been conducted on Hastelloy X. The tests were conducted at 871°C (1600°F), and the interim data are reported in Table 9. Hysteresis loops at roughly half the cycle life for two strain ranges (i.e., 2 and 0.6%) are compared with those generated without hold periods in Fig. 24, which shows for the 0.6% total strain range that tests conducted with a tensile hold time only developed a mean compressive stress and that tests conducted with a compressive hold period developed a mean tensile stress; while for a test generated with both a tensile and compressive hold, little or no mean stress was developed. Figure 24 also shows that compressive hold times tend to be the most damaging mode.

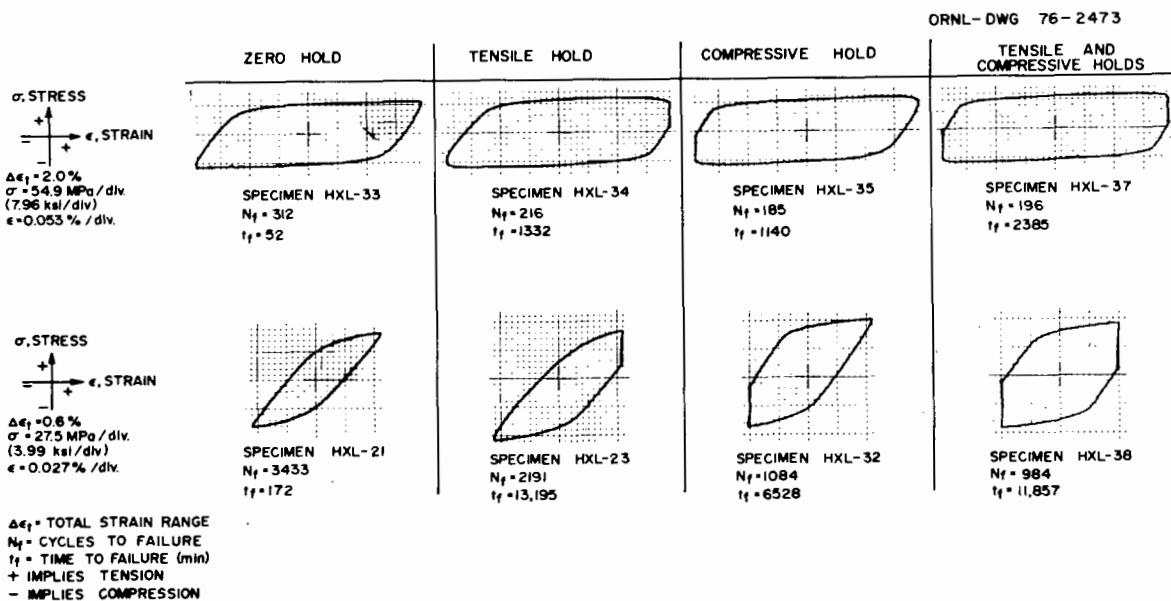


Fig. 24. Comparison of Actual Hysteresis Loops from Strain-Controlled Low-Cycle Fatigue Tests Involving Zero Hold Periods or 0.1-hr Hold Periods at Peak (Maximum, Minimum, or Both) Strain Amplitudes. Tests were conducted on Hastelloy X (Heat 2600-3-4936) at 871°C (1600°F) in air.

Lord and Coffin<sup>35</sup> characterized the low-cycle fatigue and hold-time behavior of cast Rene 80 and found that compressive hold times were more damaging than tensile hold times. They qualitatively explained this behavior in terms of the ability of the material to sustain a mean stress at cycle lives beyond the transition fatigue life; that is, the elastic strain range was greater than the plastic strain range. They postulated that in this material, compressive hold times were particularly deleterious at low strain ranges, because tensile mean stresses could be maintained which enhanced crack growth rates. For Hastelloy X tested at 871°C (1600°F), the cycle life of a continuously cycled specimen tested at 0.6% total strain range is greater than the transition fatigue life. Therefore, the above explanation as to why compressive hold times are more damaging than tensile hold times is plausible.

Plots of the inelastic strain components from tests conducted to date are given in Fig. 25. Only data in the range 649°C (1200°F) to 871°C (1600°F) are included in this plot. The  $\Delta\epsilon_{pp}$  plastic strain data obtained from tests conducted at temperatures of 538°C (1000°F) and lower were excluded from the plot, since values clearly fell above the high-temperature data.

Cyclic lines associated with the various components of time-dependent inelastic strain, that is,  $N_{cp}$ ,  $N_{pc}$ , and  $N_{cc}$ , were calculated using the interaction damage rule:<sup>36</sup>

$$\frac{F_{pp}}{N_{pp}} + \frac{F_{pc}}{N_{pc}} + \frac{F_{cp}}{N_{cp}} + \frac{F_{cc}}{N_{cc}} = \frac{1}{N_f} \quad , \quad (8)$$

where

$$F_{pp} = \Delta\epsilon_{pp} / \Delta\epsilon_{in} \quad , \quad (9)$$

$$F_{pc} = \Delta\epsilon_{pc} / \Delta\epsilon_{in} \quad , \quad (10)$$

---

<sup>35</sup>D. C. Lord and L. F. Coffin, Jr., "Low-Cycle Fatigue Hold Time Behavior of Cast Rene 80," *Metall. Trans.* 4: 1647 (1973).

<sup>36</sup>S. S. Manson, "The Challenge to Unify Treatment of High Temperature Fatigue — A Partisan Proposal Based on Strain Range Partitioning," pp. 744-75 in *Fatigue at Elevated Temperatures*, *Am. Soc. Test. Mater. Spec. Tech. Publ.* 520, ed. by A. E. Cardin, A. J. McEvily, and C. Wells, American Society for Testing and Materials, Philadelphia, 1973.

$$F_{cp} = \Delta\epsilon_{cp} / \Delta\epsilon_{in} , \tag{11}$$

$$F_{cc} = \Delta\epsilon_{cc} / \Delta\epsilon_{in} , \tag{12}$$

$\Delta\epsilon_{in}$  = total inelastic strain range associated with the particular cycle being analyzed.

Tests in air are continuing, and tests in helium will begin in the near future.

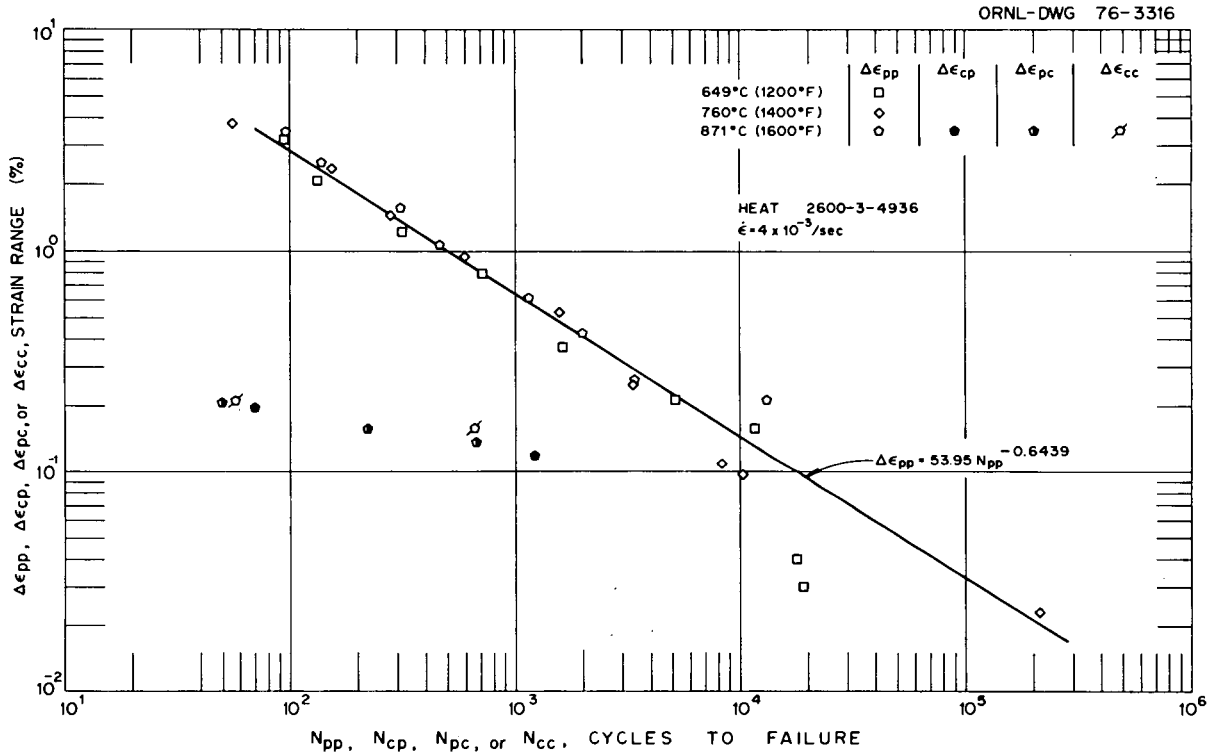


Fig. 25. Partitioned Inelastic Strain Components vs Associated Figure Lifetimes For Hastelloy X.

## SUBCRITICAL CRACK GROWTH

Numerous investigations<sup>37-41</sup> have shown that the fatigue behavior of structural alloys, specifically the crack growth rate, is dependent on the test environment in addition to the more conventional parameters of temperature, frequency, and mean stress level. To determine the effects of simulated HTGR primary coolant on the fatigue crack propagation behavior of Hastelloy X, tests were conducted in air at 25, 538, and 649°C (77, 1000, and 1200°F), and comparative tests were conducted in HTGR helium at the elevated temperatures. All tests had an  $R$  ratio (ratio of minimum to maximum stress intensity) of 0.05 and were run at a frequency of 1 Hz at the elevated temperatures and 40 Hz at room temperature, where thermally induced processes are largely inactive. The results are shown in Figs. 26-28. Data on Hastelloy X 280, a low-cobalt version of Hastelloy X, is shown for comparison at room temperature and at 538°C (1000°F).<sup>42</sup>

No difference in crack growth rate was observed in simulated HTGR helium at either of the elevated test temperatures when compared with results obtained in air with specimens of similar geometry. However, a systematic, reproducible difference was observed at all temperatures between the compact tension and the WOL specimens. A similar effect has been observed in a previous study<sup>14</sup> using the same specimen geometries. It is probably due to a slight departure from linear elastic fracture mechanics testing conditions within the small compact tension specimen in as much as an excessively large plastic zone is generated, relative to the planar specimen dimensions. Hence, the calculated value of stress intensity is not strictly valid. None the less, comparison of crack growth rates using the compact tension specimen in both air and simulated HTGR helium indicates no difference in crack growth rates as shown in Figs. 27 and 28.

Averaged results of both test geometries are given in Fig. 29 for all test temperatures. Crack growth rate is clearly shown to increase with increasing temperature at a constant level of  $\Delta k$ .

---

<sup>37</sup>H. H. Smith, P. Shahinian, and M. R. Achter, *Trans. AIME* 245: 947 (1969).

<sup>38</sup>M. R. Achter, G. J. Danek, Jr., and H. H. Smith, *Trans. AIME* 227: 1296 (1963).

<sup>39</sup>L. A. James and R. L. Knecht, "Fatigue-Crack Propagation Behavior of Type 304 Stainless Steel in a Liquid Sodium Environment," *Metall. Trans.* 6a(1): 109-16 (1975).

<sup>40</sup>L. A. James and R. L. Knecht, *Subcritical Crack Growth*, HEDL-TME 74-4, HEDL Quarterly Technical Report, 1: C13-C19 (January 1975).

<sup>41</sup>W. R. Corwin, "Subcritical Crack Growth Studies," *Mechanical Properties Test Data for Structural Materials Q. Prog. Rep. Oct. 31, 1975*, ORNL-5107, pp. 196-201.

<sup>42</sup>L. A. James, *The Effect of Temperature Upon the Fatigue-Crack Propagation Behavior of Hastelloy X-280*, HEDL-TME 76-40 (May 1976).

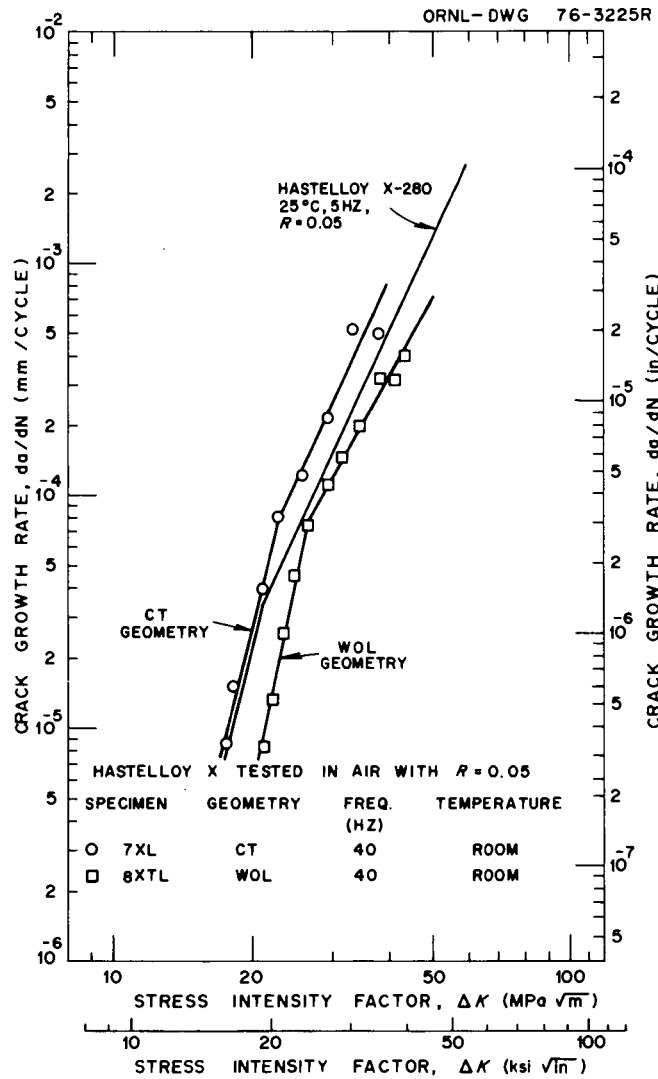


Fig. 26. Effect of Specimen Geometry on Fatigue Crack Growth Rate at Room Temperature.

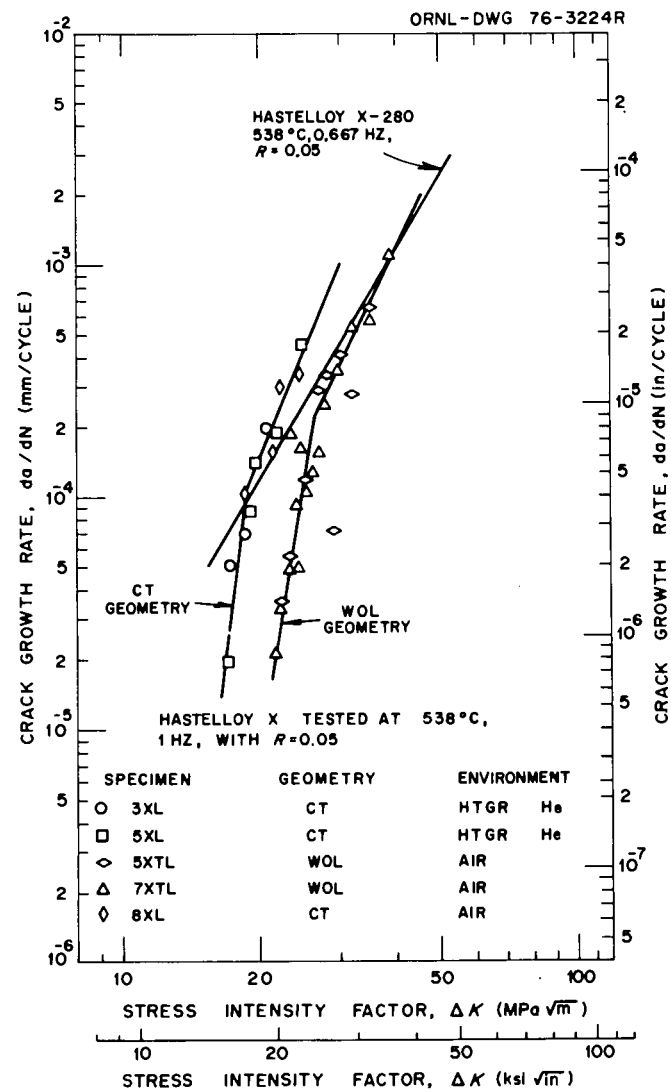


Fig. 27. Effect of Simulated HTGR Primary Coolant and Specimen Geometry on Fatigue Crack Growth Rate at 538°C (1000°F).

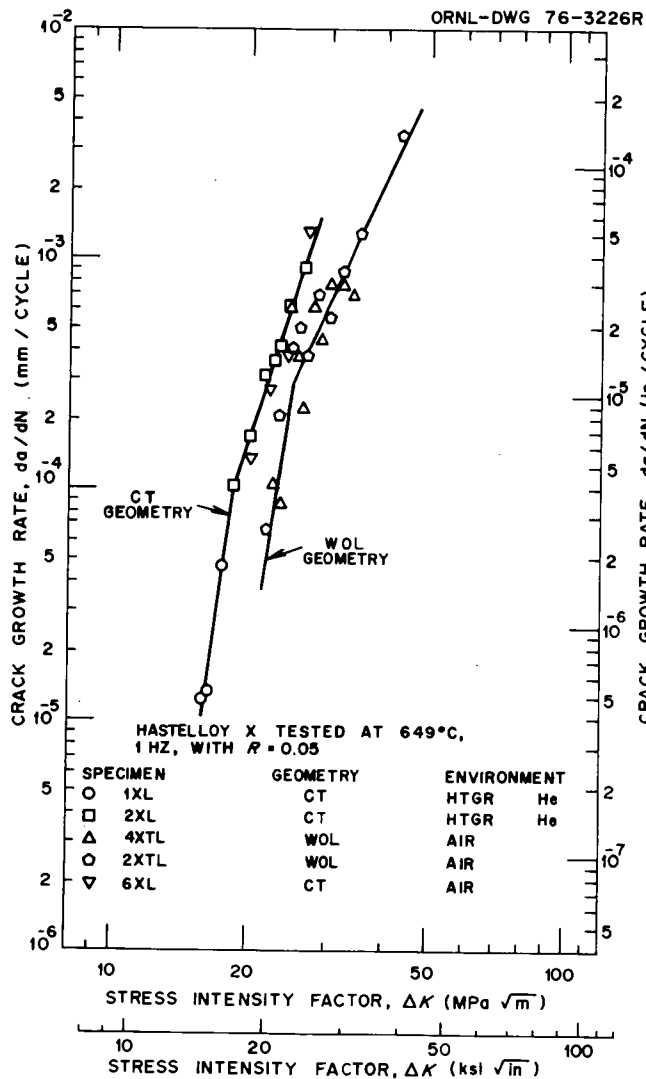


Fig. 28. Effect of Simulated HTGR Primary Coolant and Specimen Geometry on Fatigue Crack Growth Rate at 649°C (1200°F).

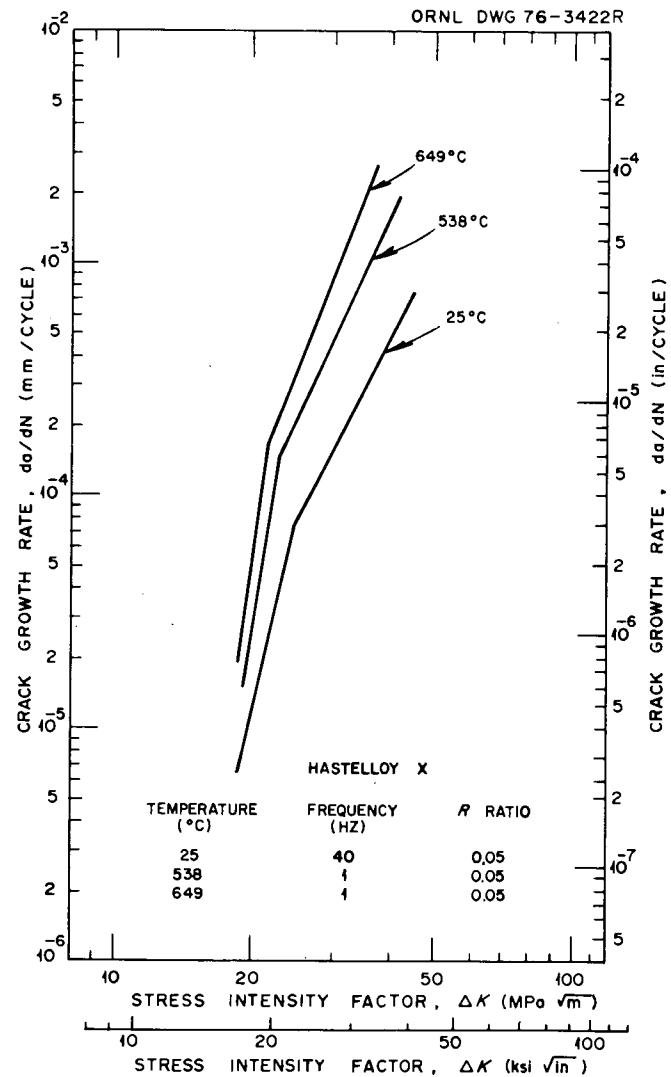


Fig. 29. Effect of Temperature on the Averaged Fatigue Crack Growth Behavior of Hastelloy X.

Results obtained at 538°C (1000°F) for Hastelloy X are compared in Fig. 30 with those for several other structural materials which are candidates for use in the HTGR and other reactor systems. The data for types 304 (ref. 43) and 316 (ref. 44) stainless steel, Inconel 718 (ref. 45) and Incoloy 800 (ref. 46) are all results obtained at 538°C (1000°F). The line of  $da/dN$  vs  $\Delta K$  for 2 1/4 Cr-1 Mo steel<sup>41</sup> was obtained by linear interpolation of results at 510 and 593°C (950 and 1100°F) and is also shown for comparison. Overall, Inconel alloy 718 shows the lower crack growth rate for most of the stress intensity values in comparison with the other materials at this temperature. The reasons for differences in crack growth rates for a given stress intensity displayed by the seven materials compared in Fig. 30 are not readily apparent. Pelloux,<sup>47</sup> in reviewing the various theories and laws of fatigue crack propagation, showed crack growth rates to be a function of many factors, including the plastic zone size and the shape at the tip of the crack, as well as the cyclic stress-strain hardening behavior of the material. In this respect, crack growth rates tend to be inversely proportional to the yield strength. Table 11 shows that at 538°C (1000°F), Inconel alloy 718 has a much higher yield strength than the other materials shown and therefore generally displays the lower crack growth rate for a given stress intensity.

#### Thermal Stability

As was indicated previously, the design lifetime of an HTGR plant is set at 280,000 hr. Therefore, the long-term elevated-temperature stability of any candidate alloy such as Hastelloy X proposed for elevated-temperature service in HTGR systems is important. Hastelloy X is a

---

<sup>43</sup>L. A. James, "Fatigue Crack Growth in Type 304 Stainless Steel Weldments at Elevated Temperatures," *J. Test. Eval.* 1(1): 52-57 (January 1973).

<sup>44</sup>L. A. James, "The Effect of Elevated Temperature upon the Fatigue-Crack Propagation Behavior of Two Austenitic Stainless Steels," pp. 341-52 in *Mechanical Behavior of Materials*, vol. III, Society of Materials Science, Japan, 1972.

<sup>45</sup>L. A. James, *Fatigue Crack Propagation Behavior of Inconel 718*, HEDL-TME 75-80 (in press).

<sup>46</sup>L. A. James, "Fatigue-Crack Growth of Incoloy 800 at Elevated Temperatures," *J. Eng. Mater. Technol.* 96(4): 249-54 (1974).

<sup>47</sup>R. M. Pelloux, "Review of Theories and Laws of Fatigue Crack Propagation," *Proceedings of the Air Force Conference on Fatigue and Fracture of Aircraft Structures and Materials*, AFFDL TR 70-144, Miami Beach, Florida, 15-18 December 1969.

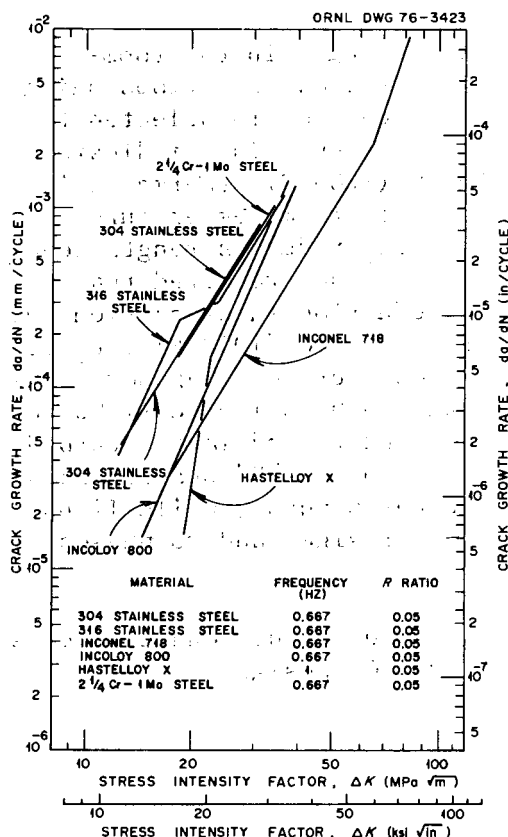


Fig. 30. Comparison of Fatigue Crack Growth Behavior of Several Candidate Structural Materials For Use in the HTGR at 538°C (1000°F).

solution-hardened alloy and as such is not expected to show large changes in mechanical properties at temperatures appropriate to HTGR design. However, the presence of molybdenum, chromium, and tungsten within the lattice may contribute to precipitation of carbides after extended periods of exposure. In an effort to determine the long-term elevated-temperature aging response of this material, samples are being exposed to high temperatures of interest to HTGR design. Following aging exposure in the unstressed conditions, tensile, creep and fatigue tests along with metallographic examination will be used to determine the magnitude and cause of any changes found. No data are yet available from this part of the program.<sup>48-51</sup>

<sup>48</sup>E. L. Wagoner, "Physical Metallurgy and Mechanical Properties of Hastelloy X," Haynes Stellite Company, Division of Union Carbide Corporation, Kokomo, Indiana, 1961.

<sup>49</sup>D. A. Yablonski, "High Temperature Fatigue Crack Propagation Behavior of Two Superalloys," Master's Thesis, Massachusetts Institute of Technology, 1976.

<sup>50</sup>G. W. Titus and W. L. Clarke, Jr., "Compatibility of Reactor Materials with High Temperature Gases," *Nucl. Eng. Des.* 24: 125-44 (1973).

<sup>51</sup>F. A. Comprelli, *High-Temperature Tensile Properties of Selected Alloys after Prolonged Thermal Exposure*, General Electric Co., GEAP-4794 (1965).

A number of investigators have reported changes in the room-temperature tensile properties of Hastelloy X following various aging treatments at elevated temperatures. Typical changes in selected tensile properties are indicated in Fig. 31. The data trend lines indicate that at temperatures in excess of about 649°C (1200°F), thermal aging may result in an initial increase or decrease in room-temperature strength. Prolonged aging treatments apparently reduce strength levels below those of the virgin material. Comprelli<sup>51</sup> has reported that increases in room-temperature strength and reduction in elongation below 15% following aging at as low a temperature as 566°C (1050°F) can occur. These changes are due to the changes in microstructure. Wagoner<sup>48</sup> has reported that aging over the temperature range 649 to 1038°C (1200 to 1900°F) resulted in the formation of grain boundary and matrix carbides of various types, including  $M_6C$ ,  $M_6C'$ ,  $M_{23}C_6$ , and an "X" phase. Comprelli reported also minor amounts of the  $AB_2$ -type Laves phase, while Titus and Clarke<sup>50</sup> have also reported the presence of sigma and mu phases in this material subsequent to aging.

Changes of the type indicated above must be further quantified as to their impact on mechanical properties for HTGR design.

#### Helium Corrosion

Hastelloy X shows superior resistance to oxidation in air, perhaps because of the unique oxidation-resistant spinel that forms as the outer layer of a duplex oxide. The long-term behavior of this material in nonoxidizing environments, however, where carburization may occur, needs to be determined. Further, static and dynamic stresses will be imposed that may influence oxidation resistance. Therefore, the surfaces of specimens are being examined as a part of this program following creep and fatigue testing. Only limited information, however, is currently available. Figures 32 and 33 show some typical photomicrographs of specimens following creep-rupture testing in helium. As expected, oxidation not only depends on the temperature but also on the stress. Figure 32 shows the specimen from test 16031 [152 MPa (22 ksi), 760°C (1400°F), 159 hr], and it exhibits a 1- $\mu$ m-thick discontinuous oxide layer on the surface and many 40- to 50- $\mu$ m-deep grain boundary penetrations in the stressed (gage) section of the specimen. The surface of the lower stressed section of the specimen (at the shoulder) was covered with a smooth, green continuous 1- $\mu$ m-thick oxide, and there was no indication of grain boundary attack. Figure 33 shows photomicrographs from test No. 16054 [62 MPa (9 ksi), 871°C (1600°F), 554 hr]. Here the surface film was very thin (<1  $\mu$ m) at the stressed part of the specimen, and there were only few 20- to 30- $\mu$ m-deep penetrations. At the unstressed part of the specimen, there was also a very thin oxide layer, and there was no indication of oxidation attack.

ORNL-DWG 76-3192

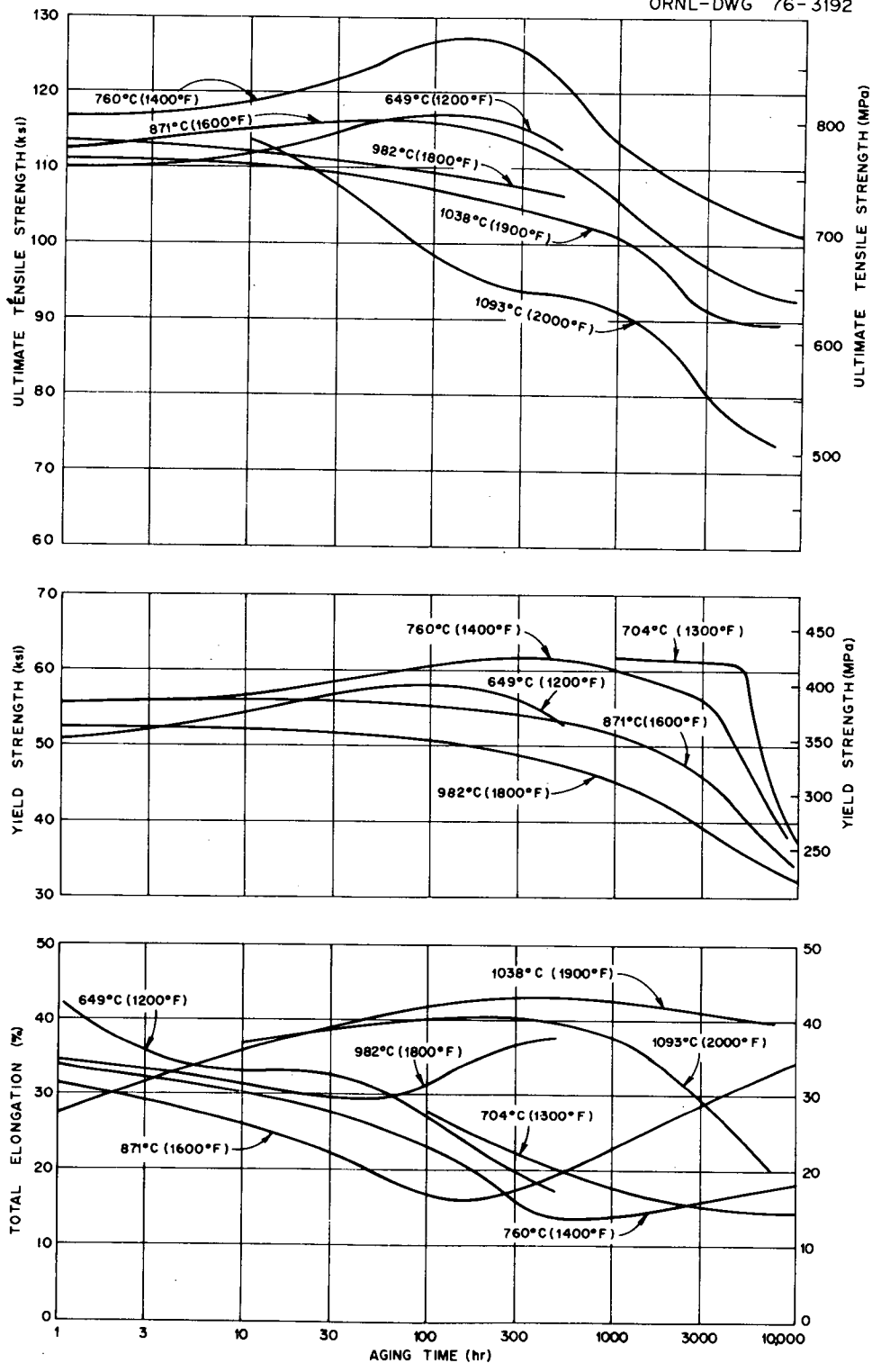
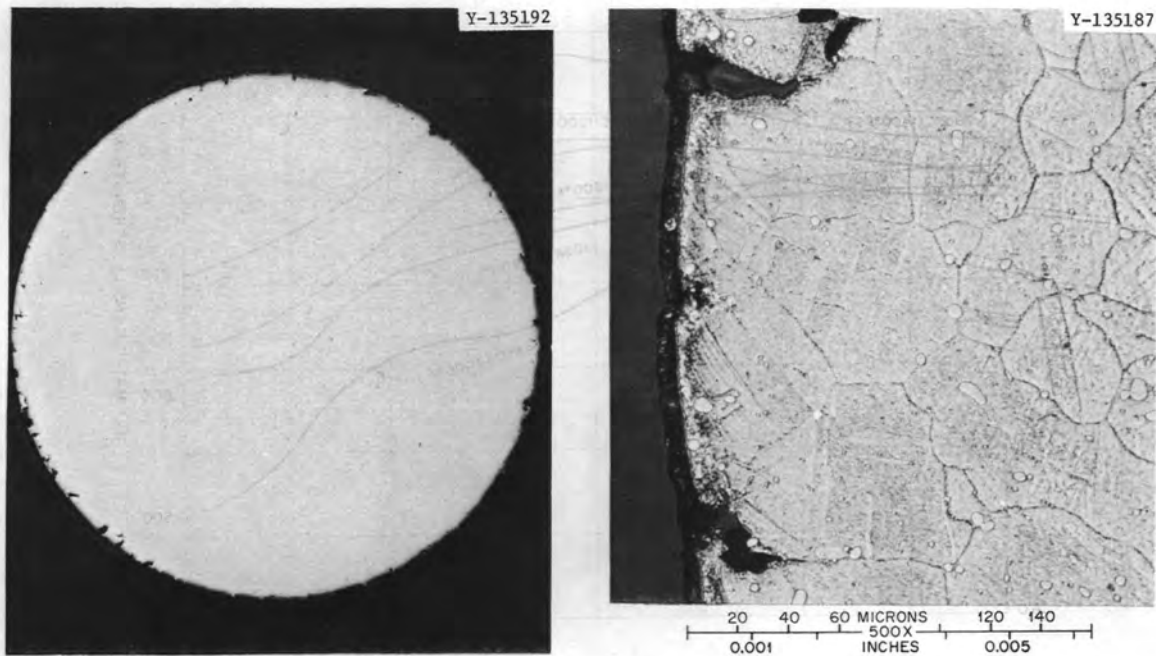
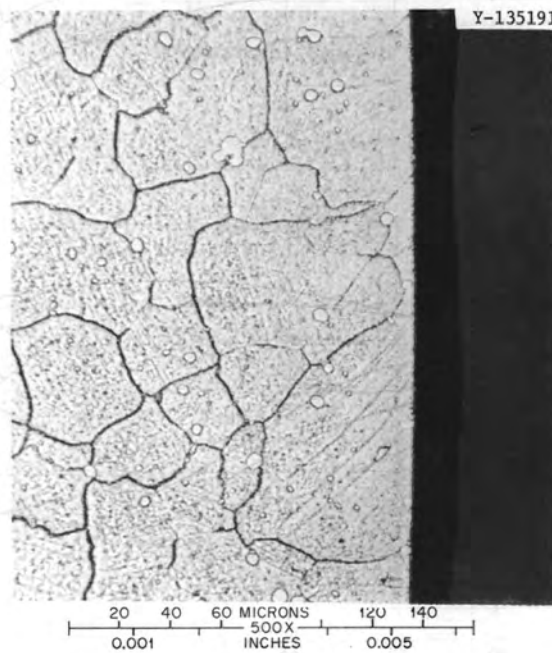


Fig. 31. Influence of Thermal Aging Time (In Air) at Several Temperatures on the Room-Temperature Tensile Properties of Hastelloy X.

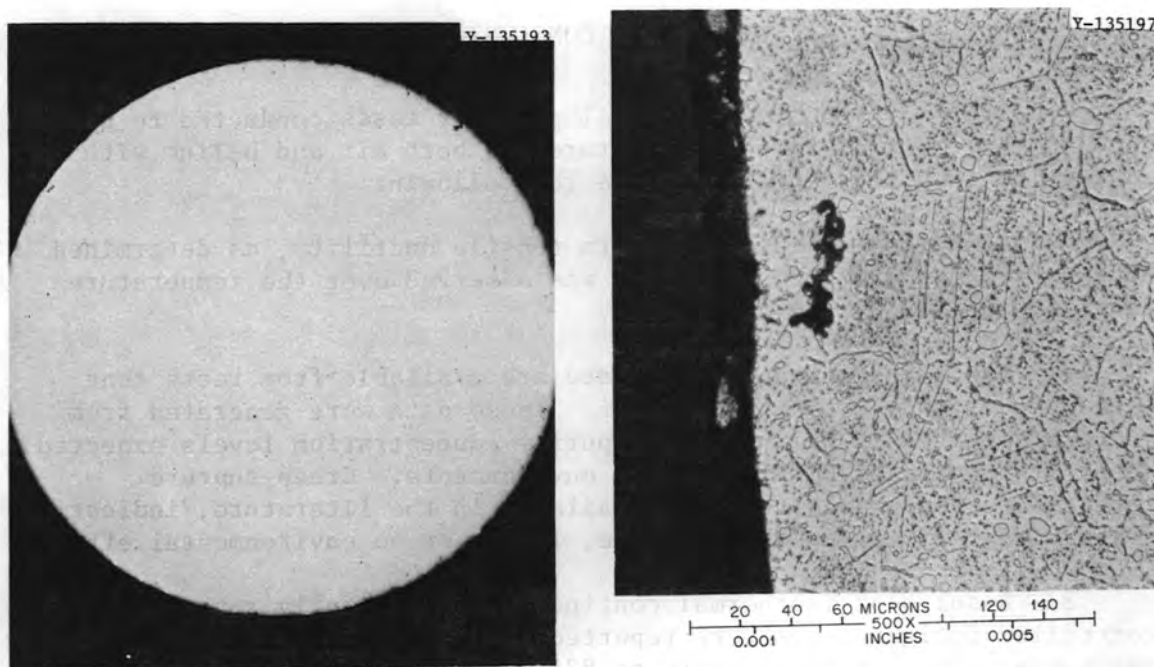


(a) Grain Boundary Penetration Along Gage Section of the Specimen. Original cross-sectional diameter of the specimen was 3.18 mm (0.125 in.).

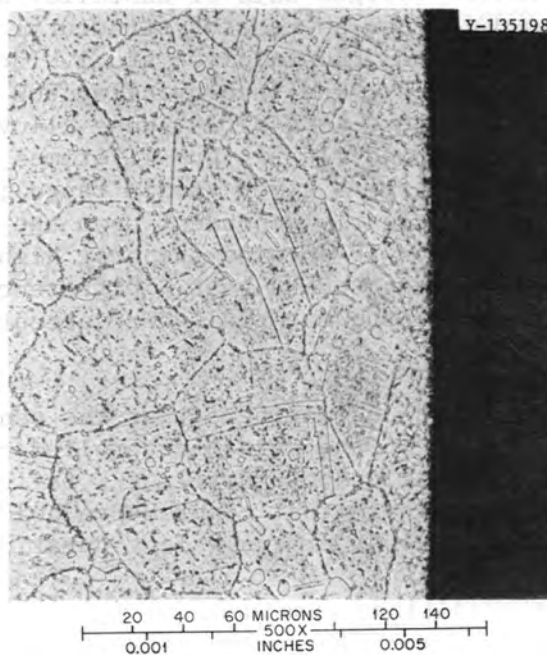


(b) Surface Edge of the Shoulder or Low Stressed Region of the Specimen.

Fig. 32. Photomicrographs of the Cross Section of Test Specimen 16031 stressed at 152 MPa (22 ksi) at 760°C (1400°F). Specimen failed after 159 hr.



(a) Surface Cross Section Along Gage Section of the Specimen.  
Original cross-sectional diameter of the specimen was 3.18 mm (0.125 in.).



(b) Surface Edge of the Shoulder or Low Stressed Region of the Specimen.

Fig. 33. Photomicrographs of the Cross Section of Test Specimen 16054 Stressed at 62 MPa (9 ksi) at 871°C (1600°F) for 554 hr.

## SUMMARY AND CONCLUSIONS

Results from interim mechanical property tests conducted to date on Hastelloy X at elevated temperatures in both air and helium with controlled impurity levels indicate the following:

1. A minimum in the short-term tensile ductility, as determined by reduction-of-area measurements, was observed over the temperature range 500 to 750°C (930 to 1380°F).
2. Creep-rupture and creep data are available from tests that have been extended to about 6500 hr. These data were generated from specimens tested in helium with impurity concentration levels expected to be prototypic of HTGR operating environments. Creep-rupture results are comparable to those available in the literature, indicating, for the test times employed to date, little or no environmental effect.
3. Results of isothermal continuous-cycling fully reversed strain-controlled fatigue tests were reported. Increasing the temperature over the range from room temperature to 871°C (1600°F) decreased the cyclic life (cycles to failure), with the largest reduction occurring between room temperature and 649°C (1200°F).
4. Comparisons were made of the best-fit curves through the fully reversed strain-controlled fatigue data of Hastelloy X and several other alloys used or proposed for use as reactor structural alloys. These alloys included types 304 and 316 stainless steel, Inconel alloy 718, 2 1/4 Cr-1 Mo steel (annealed), and Incoloy alloy 800. Comparisons were made from room temperature to 649°C. These alloys tended to generally exhibit similar low-cycle fatigue lifetimes (as determined by comparing cycles to failure for a given strain range); however, high-cycle fatigue behavior was clearly dependent upon the short-term tensile strength, with Inconel alloy 718 showing the best high-cycle fatigue resistance and Hastelloy X the second best. Differences in high-cycle fatigue resistance between these materials were accentuated by increasing the temperature.
5. Hold periods introduced during either the peak tension or compression, or both, portions of the strain-controlled cycle were found to decrease the cycles to failure of Hastelloy X fatigued in air at 871°C. Interim results indicate that compressive holds are more detrimental than tensile hold periods of equivalent duration.
6. For the test conditions examined, no difference was found between the crack growth rates of Hastelloy X in air vs those in simulated HTGR primary coolant. This might be expected because of the excellent oxidation resistance of this material over the temperature range studied. If HTGR helium does affect the fatigue crack propagation rate behavior of Hastelloy X, it will be at higher temperatures and/or lower cyclic frequencies than those investigated to date.

7. Varying the test specimen geometry was shown to have an effect on the fatigue crack growth rate of Hastelloy X tested in air. An adequate explanation of this behavior has not been made to date.

8. The fatigue crack growth rate increases monotonically with increasing temperature over the range investigated.

9. Room-temperature tensile test results available from the literature were discussed and compared with those conducted on Hastelloy X that had been aged for various times and temperatures. Aging at temperatures at or in excess of about 566°C (1050°F) generally results in an initial increase in room-temperature strength and loss of some ductility, followed by a decrease in strength. Additional elevated-temperature tests conducted on material aged for times in excess of 10,000 hr are recommended.

#### ACKNOWLEDGMENTS

The authors gratefully acknowledge the following personnel for their assistance in conducting the tests reported herein: E. Bolling, L. K. Egner, E. B. Patton, Jr., C. O. Stevens, W. B. Johnson, and R. F. Eaves. We also express our appreciation to R. B. Parker for editing the document and to Collene Trammell for typing the manuscript.



APPENDIX



Calculation of Equations Defining Fatigue Behavior of Several Materials

Given below are the equations defining cycles to failure for various strain ranges for several materials compared with Hastelloy X in Figs. 21-23. The equations give best-fit lines through strain-controlled data generated at a strain rate of  $4 \times 10^{-3}$ /sec.

2 1/4 Cr-1 Mo steel, annealed

Cycles to failure ( $N_f$ ) can be expressed as a function of total strain range ( $\Delta\epsilon_t$ , %) by

$$\log N_f = \alpha_0 + \alpha_1 \log \Delta\epsilon_t + \alpha_2 (\log \Delta\epsilon_t)^2 + \alpha_3 (\log \Delta\epsilon_t)^3, \quad (A-1)$$

where  $\alpha_0, \alpha_1, \alpha_2, \alpha_3$  are unknown constants estimated by the method of least squares:

Maximum temperature	Room temperature to 427°C (800°F)	538°C (1000°F)	593°C (1100°F)
$\alpha_0$	3.578 ± 0.044	3.302 ± 0.081	3.153 ± 0.051
$\alpha_1$	-2.358 ± 0.176	-2.388 ± 0.296	-1.803 ± 0.273
$\alpha_2$	3.506 ± 0.274	3.521 ± 0.592	2.613 ± 0.466
$\alpha_3$	-4.197 ± 0.633	-2.577 ± 1.122	-3.738 ± 1.250

Applicable for cyclic strain rates  $\approx 4 \times 10^{-3}$ /sec.

Applicable product forms: plate, pipe, bar in the annealed or isothermally annealed condition.

Data collected conformed to the following limitations:

Carbon content: 0.07-0.15 wt %  
 Chromium content: 2.0-2.5 wt %  
 Molybdenum content: 0.9-1.1 wt %  
 Minimum room temperature ultimate tensile strength: 414 MPa (60 ksi)  
 Minimum room temperature (0.2% offset) yield strength: 207 MPa  
 (30 ksi)

Notes: No attempts were made to correct for the effects of mean strain or stress.

Except for minimum carbon, these restrictions are a subset of those given in the *Nuclear Systems Materials Handbook* under ASME Spec. SA-336-F22A and SA-387-22-C1.2. Other applicable specifications permit either a wider range in chemical composition or greater minimum strength values. The minimum carbon content of 0.07% is in accordance with ASME Sect. III for components in service at about 371°C (700°F).

Inconel alloy 718, 954°C solution annealed

Room temperature

$$\log N_f = 4.317 - 4.184 \log \Delta\epsilon_t + 3.295 (\log \Delta\epsilon_t)^2 - 2.562 (\log \Delta\epsilon_t)^3, \quad (\text{A-2})$$

538°C (1000°F):

$$\log N_f = 4.590 - 8.673 \log \Delta\epsilon_t + 12.178 (\log \Delta\epsilon_t)^2 - 7.048 (\log \Delta\epsilon_t)^3, \quad (\text{A-3})$$

649°C (1200°F):

$$\log N_f = 4.082 - 7.872 \log \Delta\epsilon_t + 12.364 (\log \Delta\epsilon_t)^2 - 8.494 (\log \Delta\epsilon_t)^3 \quad (\text{A-4})$$

 $\Delta\epsilon_t$  in %Type 316 stainless steel

Room temperature:

$$\Delta\epsilon_t = \Delta\epsilon_p + \Delta\epsilon_e$$

$$\log \Delta\epsilon_p = -0.176 - 0.499 \log N_f \quad (\text{A-5})$$

$$\log \Delta\epsilon_e = -1.75 - 0.179 \log N_f \quad (\text{A-6})$$

 $\Delta\epsilon_{p,e}$ 

649°C (1200°F):

$$\Delta\epsilon_t = \Delta\epsilon_p + \Delta\epsilon_e$$

$$\log \Delta\epsilon_p = -0.264 - 0.560 \log N_f \quad (\text{A-7})$$

$$\log \Delta \epsilon_e = -1.91 - 0.153 \log N_f \quad (\text{A-8})$$

$$\Delta \epsilon_{\rho, e}$$

Type 304 stainless steel

Room temperature:

$$\Delta \epsilon_t = \Delta \epsilon_p + \Delta \epsilon_e$$

$$\log \Delta \epsilon_p = -0.608 - 0.403 \log N_f \quad (\text{A-9})$$

$$\log \Delta \epsilon_e = -1.30 - 0.303 \log N_f \quad (\text{A-10})$$

$$\Delta \epsilon_{\rho, e}$$

538 and 566°C (1000 and 1050°F):

$$\Delta \epsilon_t = \Delta \epsilon_p + \Delta \epsilon_e$$

$$\log \Delta \epsilon_p = 1.67 - 0.515 \log N_f \quad (\text{A-11})$$

$$\log \Delta \epsilon_e = 0.0704 - 0.149 \log N_f \quad (\text{A-12})$$

$$\Delta \epsilon_{\rho, e} \text{ in } \%$$

649°C (1200°F):

$$\Delta \epsilon_t = \Delta \epsilon_p + \Delta \epsilon_e$$

$$\log \Delta \epsilon_p = 0.113 - 0.681 \log N_f \quad (\text{A-13})$$

$$\log \Delta \epsilon_e = -1.88 - 0.188 \log N_f \quad (\text{A-14})$$

$$\Delta \epsilon_{\rho, e} \text{ not in } \%$$

Austenitic stainless steels, types 304, 310, 316, 347, and 348 (ref. 1)

Room temperature to 427°C (800°F):

$$\Delta\epsilon_t (\%) = 64.0 N_f^{-0.5} + 0.223 \quad (\text{A-15})$$

Incoloy alloy 800, grades 2 and H

Room temperature:

$$\begin{aligned} \log N_f = & 3.903 - 2.903 \log \Delta\epsilon_t + 0.831 (\log \Delta\epsilon_t)^2 \\ & - 0.177 (\log \Delta\epsilon_t)^3 \end{aligned} \quad (\text{A-16})$$

538°C (1000°F):

$$\begin{aligned} \log N_f = & 3.485 - 2.391 \log \Delta\epsilon_t + 2.272 (\log \Delta\epsilon_t)^2 \\ & - 3.009 (\log \Delta\epsilon_t)^3 \end{aligned} \quad (\text{A-17})$$

649°C (1200°F):

$$\begin{aligned} \log N_f = & 3.191 - 2.099 \log \Delta\epsilon_t + 1.495 (\log \Delta\epsilon_t)^2 \\ & - 1.295 (\log \Delta\epsilon_t)^3 \end{aligned} \quad (\text{A-18})$$

 $\Delta\epsilon_t$  in %AISI 1010 steel

Room temperature:

$$\log N_f = 3.710 - 2.706 \log \Delta\epsilon_t + 1.910 (\log \Delta\epsilon_t)^2 \quad (\text{A-19})$$

538°C (1000°F):

$$\log N_f = 3.320 - 1.410 \log \Delta\epsilon_t + 1.670 (\log \Delta\epsilon_t)^2 \quad (\text{A-20})$$

---

<sup>1</sup>Personal communication from C. E. Jaske, Battelle Columbus Laboratory, June 16, 1975.

649°C (1200°F):

$$\log N_f = 3.250 - 1.280 \log \Delta \epsilon_t + 0.681 (\log \Delta \epsilon_t)^2 \quad (\text{A-21})$$

$\Delta \epsilon_t$  in %

U.S.

ORNL/TM-5405  
Distribution  
Category UC-77

## INTERNAL DISTRIBUTION

1-2.	Central Research Library	57.	C. T. Liu
3.	Document Reference Section	58.	E. L. Long, Jr.
4-13.	Laboratory Records Department	59.	A. L. Lotts
14.	Laboratory Records, ORNL RC	60.	A. P. Malinauskas
15.	ORNL Patent Office	61.	W. R. Martin
16.	R. J. Beaver	62.	H. E. McCoy
17.	M. K. Booker	63.	H. C. McCurdy
18-27.	C. R. Brinkman	64.	C. J. McHargue
28.	J. P. Callahan	65.	R. K. Nanstad
29.	D. A. Canonico	66.	J. P. Nichols
30.	J. H. Coobs	67.	P. Patriarca
31.	J. M. Corum	68.	S. Peterson
32-34.	W. R. Corwin	69.	H. Postma
35.	F. L. Culler	70.	C. E. Pugh
36.	J. E. Cunningham	71.	P. L. Rittenhouse
37.	J. H. DeVan	72.	T. K. Roche
38-40.	J. R. DeStefano	73.	R. Salmon
41.	R. G. Donnelly	74.	J. P. Sanders
42.	G. G. Fee	75.	J. L. Scott
43.	B. L. Greenstreet	76.	V. K. Sikka
44.	J. C. Griess, Jr.	77.	G. M. Slaughter
45.	J. P. Hammond	78-85.	J. P. Strizak
46.	W. O. Harms	86.	D. B. Trauger
47-49.	M. R. Hill	87.	J. R. Weir, Jr.
50.	J. M. Holmes	88.	G. D. Whitman
51.	H. Inouye	89.	P. M. Brister (consultant)
52.	P. R. Kasten	90.	John Moteff (consultant)
53.	J. F. King	91.	Hayne Palmour III (consultant)
54.	R. T. King	92.	J. W. Prados (consultant)
55.	R. L. Klueh	93.	N. E. Promisel (consultant)
56.	K. C. Liu	94.	D. F. Stein (consultant)

## EXTERNAL DISTRIBUTION

95-96. USERDA DIVISION OF NUCLEAR RESEARCH AND APPLICATIONS,  
Washington, DC 20545

Director

97-98. USERDA DIVISION OF NUCLEAR FUEL CYCLE AND PRODUCTION,  
Washington, DC 20545

99-100. USERDA OAK RIDGE OPERATIONS OFFICE, P.O. Box E, Oak Ridge,  
TN 37830

Director, Reactor Division

Director, Research and Technical Support Division

101-267. USERDA TECHNICAL INFORMATION CENTER, Office of Information  
Services, P.O. Box 62, Oak Ridge, TN 37830

For distribution as shown in TID-4500 Distribution Category,  
UC-77 (Gas-Cooled Reactor Technology)